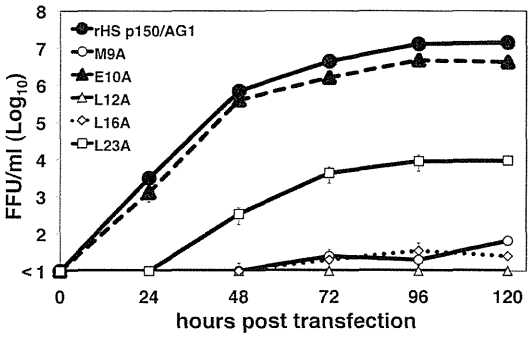

FIG 4 The self-interacting capacity of the N-terminal region of the capsid protein is essential for efficient virus production. BHK cells were transfected with *in vitro*-synthesized genomic RNA of wild-type RV or the capsid protein mutant RVs, and the viral titers in media harvested at the indicated times were determined with FFA. The averages from two independent experiments are presented. Error bars indicate the range of values in the two experiments.

AG1. In contrast, $^{FLAG}C_{1-300}$-E10A, which can interact with ^{AG1}p150, colocalized with p150/AG1 to form filamentous structures, as observed for $^{FLAG}C_{1-300}$. These results indicate that the self-interacting capacity of C_{1-30} is important for the capsid-p150 interaction and the colocalization of the capsid protein with the filamentous p150 structures in cells.

The self-interacting N-terminal region of the capsid protein is essential for RV replication. M9A, E10A, L12A, L16A, and L23A were also introduced into the genome of rHS-p150/AG1. The virus life cycle was initiated from transfected viral RNAs synthesized *in vitro*, and the viral titers in the culture supernatants were analyzed. The viral titer of rHS-p150/AG1 containing E10A (rHS-p150/AG1-E10A) was similar to that of the parental rHS-p150/AG1 (Fig. 4). In contrast, the viral titers of rHS-p150/AG1 containing M9A, L12A, L16A, or L23A (rHS-p150/AG1-E10A, -L12A, -L16A, or -L23A, respectively) were severely reduced, although the effect of L23A was smaller than the effects of M9A, L12A, and L16A (Fig. 4). These data show that the self-interacting N-terminal region of the capsid protein is essential for efficient viral replication.

Self-interacting N-terminal region of the capsid protein is required for the capsid activity that enhances viral gene expression. Tzeng et al. (17) reported that the eight residues at the N terminus of the capsid protein are required to promote viral RNA synthesis. Therefore, we analyzed the correlation between the self-interacting capacity of the capsid protein and its viral-gene-expression-promoting activity. HS-Rep-P2R is a subgenomic replicon RNA containing a unit of the P2R reporter gene that encodes the luciferase gene instead of the SP gene (Fig. 5A). BHK cells were transfected with HS-Rep-P2R alone or together with plasmid encoding C_{1-300}, $^{FLAG}C_{1-300}$, $^{FLAG}C_{51-300}$, or $^{FLAG}C_{1-300}$-20P21, -M9A, -E10A, -L12A, -L16A, or -L23A. A mutant replicon with defective RdRp catalytic activity (HS-Rep-GND-P2R) was used as the control. In the absence of capsid expression (Fig. 5B, empty), the luciferase activity of HS-Rep-P2R was as low as that of HS-Rep-GND-P2R. In the presence of C_{1-300} or $^{FLAG}C_{1-300}$, the luciferase activity of HS-Rep-P2R increased ~10^4-fold. This effect was not observed in cells transfected with HS-Rep-GND-P2R. $^{FLAG}C_{1-300}$ and $^{FLAG}C_{1-300}$-E10A enhanced the luciferase activity of HS-Rep-P2R (Fig. 5B), whereas $^{FLAG}C_{51-300}$ and $^{FLAG}C_{1-300}$-20P21, -M9A, -L12A, -L16A, and -L23A showed no or reduced enhancement of the luciferase activity (Fig. 5B). Of these mutants, $^{FLAG}C_{1-300}$-L23A showed moderate activity, but it was still very much lower (~10%) than those of C_{1-300}, $^{FLAG}C_{1-300}$, and $^{FLAG}C_{1-300}$-E10A (Fig. 5B). Similar to the luciferase activities, the fluorescent signals of p150/AG1 were detected in cells expressing HS-Rep-P2R together with $^{FLAG}C_{1-300}$, $^{FLAG}C_{1-300}$-E10A, or $^{FLAG}C_{1-300}$-L23A but not in those expressing $^{FLAG}C_{51-300}$ or $^{FLAG}C_{1-300}$-20P21, -M9A, -L12A, or -L16A (Fig. 5D).

The self-interacting N-terminal region of the capsid protein is not essential for VLP production but is essential for VLP infectivity. To determine whether virion formation was affected by the mutations in the N-terminal region of the capsid protein, the efficiency of VLP production by an SP-encoding plasmid expressing a mutant capsid protein was analyzed. SP/C_{1-300}, SP/C_{51-300}, and SP/C_{1-300} carrying 20P21, M9A, E10A, L12A, L16A, or L23A (SP/C_{1-300}-20P21, -M9A, -E10A, -L12A, -L16A, or -L23A, respectively) were evaluated. BHK-HS-Rep cells constitutively express an RV subgenomic replicon encoding a puromycin resistance gene in place of the SP genes (Fig. 6A). Fluorescence microscopy and immunoblotting showed that BHK-HS-Rep cells expressed p150/AG1 and p90 (Fig. 6B and C). These cells were transfected with plasmids encoding SPs (capsid, E1, and E2), and the titers of the infectious VLPs in the culture supernatants were measured at 48 hpt. The infectious titers of VLPs were measured with FFA. The titers of infectious VLPs carrying SP/C_{51-300} or SP/C_{1-300}-20P21, -M9A, -L12A, -L16A, or -L23A were 100- to 1,000-fold lower than those carrying SP/C_{1-300} or SP/C_{1-300}-E10A (Fig. 6D). The physical amounts of VLPs, which were either infectious or noninfectious, were also evaluated. The VLPs released into the culture supernatants were pelleted with sucrose-cushioned centrifugation, and the viral antigens (E1 and capsid) in the pellets were detected with immunoblotting (Fig. 6E, sup). Despite the large differences in the infectious titers, the total amounts of VLPs released into the supernatants were equivalent for the viruses encoding different

and the input samples were analyzed by immunoblotting with an anti-Myc antibody (for $^{myc}C_{1-30}$ constructs) or an anti-FLAG antibody (for $^{FLAG}C_{1-30}$ constructs). The panel shows data representative of results from three independent experiments. (C) Coimmunoprecipitation assays of a series of $^{FLAG}C_{1-30}{}^{mC}$ mutants with ^{AG1}p150. 293T cells were cotransfected with plasmids expressing the series of $^{FLAG}C_{1-30}{}^{mC}$ constructs and ^{AG1}p150. The precipitates bound to anti-FLAG beads and the input samples were analyzed by immunoblotting with an anti-AG1 antibody (for ^{AG1}p150) or an anti-FLAG antibody (for $^{FLAG}C_{1-30}{}^{mC}$). The panel shows data representative of results from three independent experiments. (D) Coimmunoprecipitation assay of the series of $^{FLAG}C_{1-300}$ mutants with ^{AG1}p150. 293T cells were cotransfected with plasmids expressing the series of $^{FLAG}C_{1-300}$ constructs ($^{FLAG}C_{1-300}{}^{mC}$ or $^{FLAG}C_{1-300}{}^{mC}$-20P21, -M9A, -E10A, -L12A, -L16A, or -L23A) and ^{AG1}p150. Coimmunoprecipitation assay and immunoblotting were performed as described in the legend to panel C. The panel shows data representative of results from three independent experiments. (E) Intracellular distributions of the series of capsid proteins (red) and p150/AG1 (green) after DNA transfection. The top left and right panels indicate the intracellular distributions of C_{1-300} and p150/AG1, respectively, in singly transfected Vero cells. The lower panels show the intracellular distributions of the series of mutant capsid proteins in the presence of p150/AG1. At 48 hpt, the cells were analyzed with IIFAs using an anticapsid antibody (for C_{1-300}) or an anti-FLAG antibody (for the series of $^{FLAG}C_{1-300}$ constructs). Nuclei were stained with DAPI (blue).

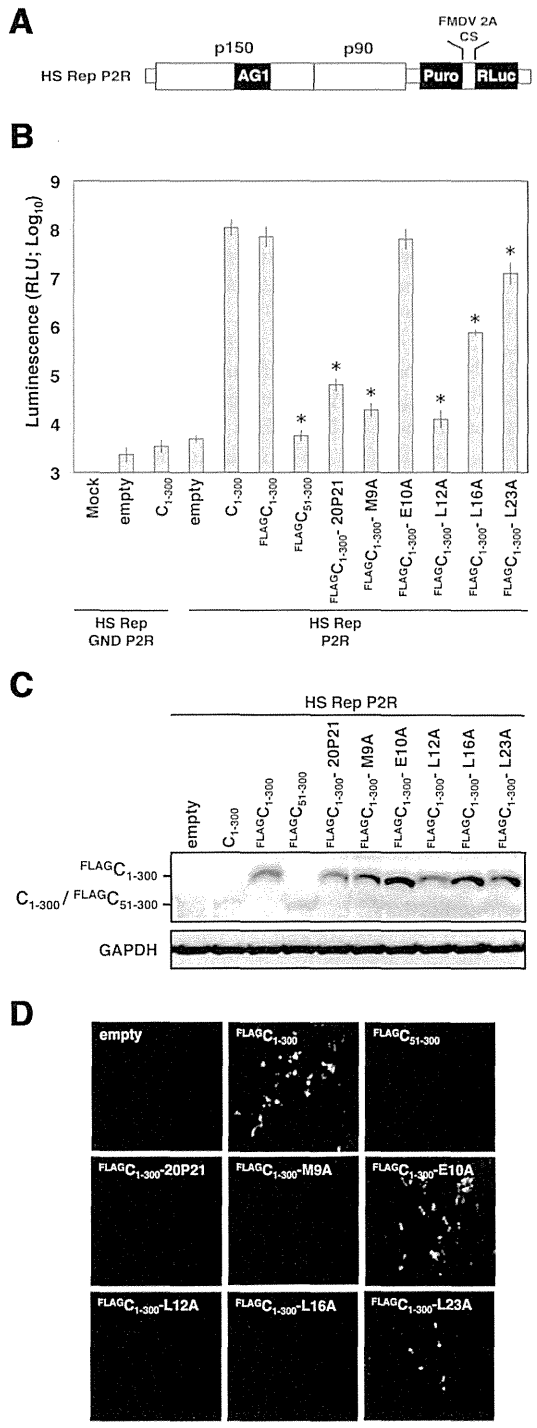

FIG 5 The viral-gene-expression-promoting activity of the capsid protein is dependent on its self-interacting N-terminal region. (A) A schematic diagram of the RV subgenomic replicon used in the reporter assays. HS-Rep-P2R was constructed by replacing the structural protein genes of rHS-p150/AG1 with the P2R reporter gene. The P2R reporter protein contained the puromycin resistance gene (*Puro*), the foot-and-mouth disease virus protease 2A cleavage sequence (FMDV 2A CS), and the *Renilla* luciferase gene (*Rluc*). FMDV 2A CS allows the dissociation of the polyprotein into Puro and Rluc. (B) *Renilla* luciferase activities derived from the subgenomic replicon. BHK cells were transfected with the subgenomic replicon RNAs together with the wild-type or mutant capsid protein mRNAs. At 72 hpt, the *Renilla* luciferase activity in the cells was measured. The averages from three independent experiments are presented. Error bars indicate standard deviations. Student *t* tests were used to determine significant differences between $^{FLAG}C_{1-300}$ and mutant capsid constructs. *, $P < 0.01$. (C) Expression of the capsid proteins in cells transfected with the series of capsid protein mRNAs. The expression of the capsid protein in the samples in panel B was confirmed by immunoblotting with anti-RV virion antibody. (D) Expression of p150/AG1 in cells containing the RV subgenomic replicon. The fluorescent signals of p150/AG1 were observed at 72 hpt, immediately before the *Renilla* luciferase activities were measured.

capsid proteins (Fig. 6E, sup). These data demonstrate that the self-interacting N-terminal region of the capsid protein is essential for infectious VLP production. To confirm the integrity of the VLPs, the VLPs produced with SP/C_{1-300} and SP/C_{1-300}-L12A (VLP-wt and VLP-L12A, respectively) were fractionated with sucrose-gradient centrifugation. VLP-L12A was used as a representative mutant producing noninfectious VLPs. The sedimentation profile of VLP-L12A was indistinguishable from that of VLP-wt (Fig. 6F). The peak fraction of genomic RNA incorporated in VLP-L12A was similar to that incorporated in VLP-wt (Fig. 6G). Thus, the self-interacting N-terminal region of the capsid protein is not essential for VLP production but is essential for VLP infectivity.

DISCUSSION

Accumulating evidence shows that the capsid proteins of many plant and animal positive-strand RNA viruses have nonstructural regulatory functions and modulate viral replication. For example, norovirus VP1 modulates RNA synthesis by interacting with the RdRp unit (27). The coronavirus N protein supports efficient RNA transcription via its chaperone activity (28, 31). The alphavirus capsid protein facilitates genomic and subgenomic RNA replication (29). The alfalfa mosaic virus coat protein activates viral RNA synthesis by conjugating the viral RNA to the RdRp unit (30, 32).

The data from the present study demonstrate that the RV capsid protein interacts with p150 via the short N-terminal region of the capsid protein.

The COILS program (http://www.ch.embnet.org/software/COILS_form.html) predicted that the N-terminal region at amino acid positions 9 to 29 forms an α-helix that adopts a coiled-coil structure. The coiled coil is a common structure that typically consists of two to five supercoiled α-helices (33, 34). The residues at positions *a* and *d* of a heptad repeat form a hydrophobic interface, and the charged amino acid residues at positions *e* and *g* participate in the stabilization of the structure via ionic interactions (33, 34). Coiled-coil domains are found in many viral proteins and are involved in protein-protein interactions mediated by helical interactions (26, 35–39). The present study indicates that the N-terminal region of the capsid protein interacts with itself. Furthermore, a helix-breaking proline insertion (20P21) or alanine substitutions at the residues predicted to be located at the hydrophobic interface (M9A, L12A, L16A, and L23A) affected this self-interaction. Therefore, our data suggest that the N-terminal region forms a homo-oligomerized coiled-coil structure. The capsid protein can form dimers via its C-terminal region (40, 41). However, it remains unclear whether the N-terminal region forms dimers or larger multimers. The capsid protein and p150 are unlikely to form a hetero-oligomerized coiled-coil structure because

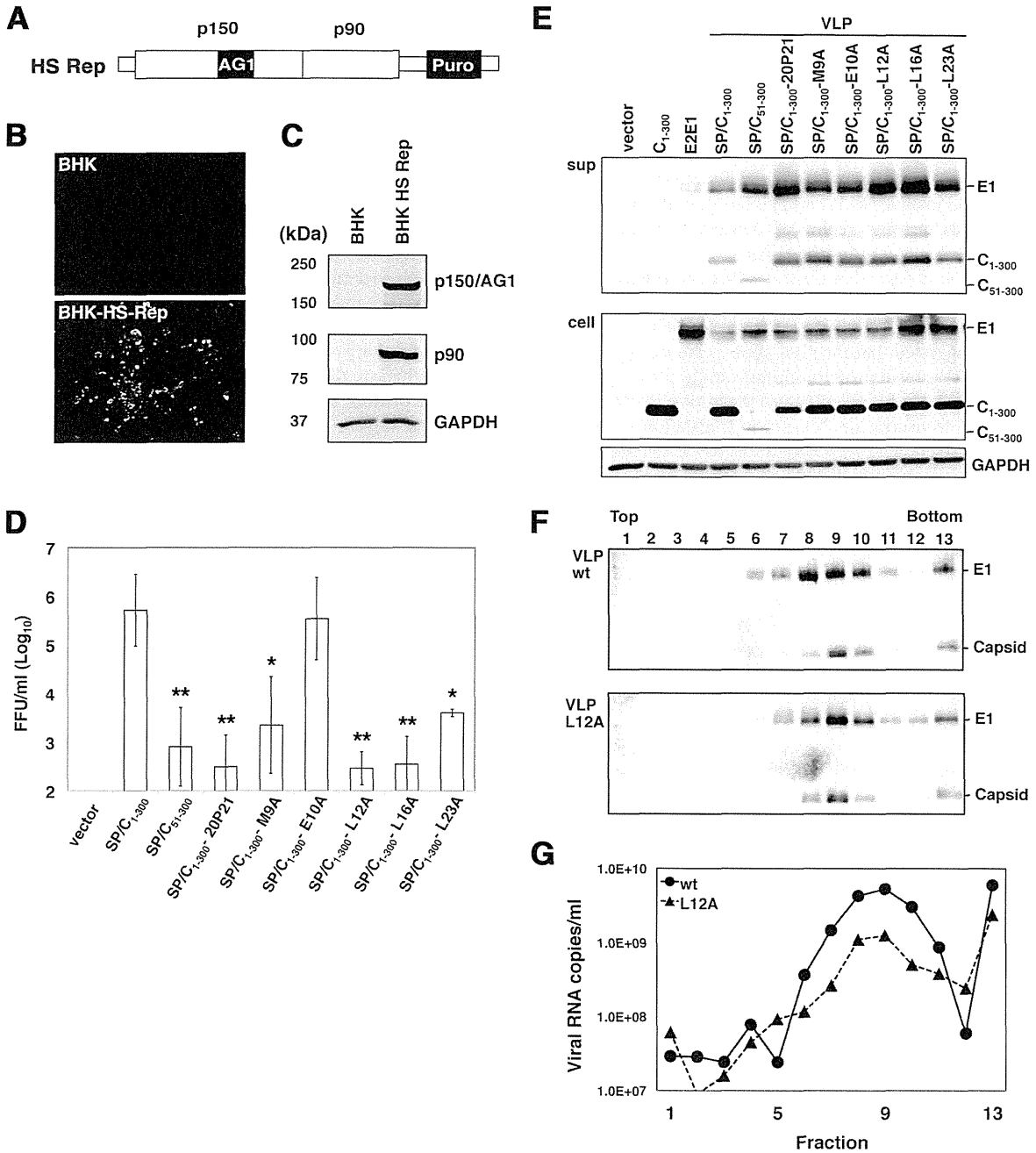

FIG 6 The self-interacting capacity of the N-terminal region of the capsid protein is responsible for virion infectivity but is not essential for virion formation. (A) A schematic diagram of the RV subgenomic replicon. The subgenomic replicon, HS Rep, was constructed by replacing the structural genes of rHS-p150/AG1 with a puromycin resistance gene (*Puro*). (B and C) BHK cells stably carrying the RV subgenomic replicon. The p150/AG1 signal was observed with fluorescence microscopy (B), and p150/AG1 and p90 were detected by immunoblotting with anti-p150 and anti-p90 antibodies, respectively (C). (D) Titers of infectious VLPs released from BHK-HS-Rep cells after transfection with the *SP* gene. BHK-HS-Rep cells were transfected with plasmids expressing the structural proteins, including the wild-type or mutant capsid protein (SP/C_{1-300}, SP/C_{1-250}, or SP/C_{1-300}-M9A, -E10A, -L12A, -L16A, or -L23A). The VLP titers in the culture media harvested at 48 hpt were determined with FFA. The means from three independent experiments are presented. Error bars indicate standard deviations. Student *t* tests were used to determine significant differences between SP/C_{1-300} and mutant SP constructs. *, $P < 0.05$; **, $P < 0.01$. (E) VLP precipitation with sucrose-cushioned ultracentrifugation. BHK-HS-Rep cells were transfected with expression plasmids encoding the capsid protein (C_{1-300}), the two spike proteins E2 and E1 (E2E1), or the structural polyproteins (C, E2, and E1) with mutations in the capsid protein. The expression levels of the structural proteins in the transfected cells were confirmed by immunoblotting with anti-RV virion and anti-GAPDH antibodies. (F and G) The VLPs derived from the wild-type capsid protein or the L12A mutant were fractionated by sucrose-gradient ultracentrifugation. The E1 and capsid proteins in the individual fractions were detected by immunoblotting with an anti-RV virion antibody. (F) The panel shows data representative of results from two independent experiments. (G) The copy numbers of the genomic RNA in the fractions were measured with qRT-PCR.

a truncated form of p150 ($p150_{1-438}$), lacking its predicted coiled-coil domains, retained the ability to interact with the capsid protein. Based on these observations, two plausible models of the interaction between the capsid protein and p150 can be proposed. In one, p150 directly recognizes the coiled-coil N-terminal region of the capsid protein. Similar modes are found in the interactions between the influenza A virus NS1 protein and the phosphoinositide 3-kinase p85-beta subunit (42) and between the yeast mitochondrial fission proteins Mdv1 and Fis1 (43). In the other model, the coiled-coil N-terminal region of the capsid protein interacts with unknown host p150-binding factors.

The present study also demonstrates that two functions of the capsid protein (its p150-interacting capacity and its viral-gene-expression-promoting activity) are closely correlated. Previous reports have suggested that the viral-gene-expression-promoting activity of the RV capsid protein is important in the early steps of RV infection, including viral entry and the initiation of viral RNA replication and transcription, but not in translation (15–18, 44–46). Upon transfection of the subgenomic RNA, the level of viral gene expression was marginal in the absence of capsid expression. However, expression of the capsid protein is not critical for viral gene expression, because viral genome replication and gene expression were maintained at high levels in cells stably carrying the subgenomic RNA but lacking capsid expression (data not shown and Fig. 6A to C). These data imply that the capsid protein is required for the initiation of viral RNA replication but not for its maintenance. p150 interacts with both p90 and the capsid protein (9, 17, 47), and p150 and p90 are thought to form the replication complex, together with the genomic RNA (8–10). The capsid protein can also bind the genomic RNA through amino acid residues 28 to 56 (48), immediately downstream from the putative coiled-coil domain. Consistent with these findings, the capsid protein may facilitate the formation of the replication complex by recruiting the genomic RNA to p150 via the N-terminal region of the capsid protein. Another possibility is that the RV capsid protein has RNA chaperone activity that promotes viral RNA replication, as observed for the coronavirus capsid protein (28, 31). Because the RV genome has the highest G+C content ever found in the positive-strand RNA viruses, this activity may be important for unwinding misfolded RNA structures.

Coiled-coil domains are also predicted in the N-terminal regions of the capsid proteins of viruses in the genus *Alphavirus*, another genus in the same family (*Togaviridae*) as RV (26, 49). In the Sindbis virus, this domain of the capsid protein plays a crucial role in nucleocapsid formation (25, 26, 29, 50–53). However, VLP production with RV mutant capsid proteins lacking the self-interacting capacity of the N-terminal region, presumably caused by the loss of the coiled coil, was similar to that of the VLP-wt. It has also been reported that, unlike those of the alphaviruses, RV VLPs are efficiently produced by the expression of only SPs in the absence of genomic RNA (54). Furthermore, the dimerization of the RV capsid protein is strengthened with an intermolecular disulfide (S-S) interaction (41), and the C-terminal half of the molecule is sufficient for this dimerization (40). Together with these reports, our study demonstrates that the role of the N-terminal region of the capsid protein in nucleocapsid formation differs markedly between the alphaviruses and RV. However, mutations affecting the N-terminal self-interaction of the RV capsid protein severely reduced the infectivity of the VLPs produced, although the sedimentation profiles of the viral proteins and genomic RNAs of the VLPs produced by a representative mutant capsid protein lacking N-terminal self-interaction were identical to those of the wild-type VLPs. Although the mechanisms underlying this loss of infectivity were not determined in this study, there are three possible explanations: (i) the N-terminal self-interacting region plays a role in the "functional" incorporation of the genomic RNA into the virion, and an inappropriately incorporated genome is not recognized by the replication components in infected cells; (ii) the self-interacting N-terminal region is required for viral uncoating, and the mutant VLPs do not release the genome into the cytoplasm of infected cells; (iii) the capsid protein incorporated into VLPs directly promotes the initiation of viral gene expression. The third hypothesis may be supported by our finding that the infectious titers of VLPs were closely related to the gene-expression-promoting activity of the capsid protein.

In conclusion, the data presented here demonstrate that the RV capsid protein associates with p150 via the self-interacting N-terminal region of the capsid protein and that the capsid protein promotes viral gene expression through its association with p150. The self-interacting N-terminal region is not essential for VLP production but is critical for VLP infectivity. This study provides important insights into the regulation of RV RNA replication by the cooperative actions of the capsid protein and p150.

ACKNOWLEDGMENTS

We thank Tero Ahola for providing the polyclonal antibody against the RV p150 protein. We also thank Hitoshi Abo for his excellent technical assistance with the sequence analyses.

This work was supported by a grant from the Japan Society for the Promotion of Science (Grant-in-Aid for Young Scientists [A], 23689028).

REFERENCES

1. **Chantler J, Wolinsky JS, Tingle A.** 2001. Rubella virus, p 963–990. *In* Knipe DM, Howley PM (ed), Fields virology, 4th ed Lippincott Williams & Wilkins, Philadelphia, PA.
2. **Chen JP, Strauss JH, Strauss EG, Frey TK.** 1996. Characterization of the rubella virus nonstructural protease domain and its cleavage site. J. Virol. **70**:4707–4713.
3. **Yao J, Yang D, Chong P, Hwang D, Liang Y, Gillam S.** 1998. Proteolytic processing of rubella virus nonstructural proteins. Virology **246**:74–82. http://dx.doi.org/10.1006/viro.1998.9179.
4. **Rozanov MN, Koonin EV, Gorbalenya AE.** 1992. Conservation of the putative methyltransferase domain: a hallmark of the 'Sindbis-like' supergroup of positive-strand RNA viruses. J. Gen. Virol. **73**(Part 8):2129–2134.
5. **Marr LD, Wang CY, Frey TK.** 1994. Expression of the rubella virus nonstructural protein ORF and demonstration of proteolytic processing. Virology **198**:586–592. http://dx.doi.org/10.1006/viro.1994.1070.
6. **Kamer G, Argos P.** 1984. Primary structural comparison of RNA-dependent polymerases from plant, animal and bacterial viruses. Nucleic Acids Res. **12**:7269–7282. http://dx.doi.org/10.1093/nar/12.18.7269.
7. **Gros C, Wengler G.** 1996. Identification of an RNA-stimulated NTPase in the predicted helicase sequence of the rubella virus nonstructural polyprotein. Virology **217**:367–372. http://dx.doi.org/10.1006/viro.1996.0125.
8. **Liang Y, Gillam S.** 2000. Mutational analysis of the rubella virus nonstructural polyprotein and its cleavage products in virus replication and RNA synthesis. J. Virol. **74**:5133–5141. http://dx.doi.org/10.1128/JVI.74.11.5133-5141.2000.
9. **Matthews JD, Tzeng WP, Frey TK.** 2009. Determinants of subcellular localization of the rubella virus nonstructural replicase proteins. Virology **390**:315–323. http://dx.doi.org/10.1016/j.virol.2009.05.019.
10. **Matthews JD, Tzeng WP, Frey TK.** 2010. Analysis of the function of cytoplasmic fibers formed by the rubella virus nonstructural replicase proteins. Virology **406**:212–227. http://dx.doi.org/10.1016/j.virol.2010.07.025.

11. Marr LD, Sanchez A, Frey TK. 1991. Efficient *in vitro* translation and processing of the rubella virus structural proteins in the presence of microsomes. Virology **180**:400–405. http://dx.doi.org/10.1016/0042-6822(91)90046-E.
12. Oker-Blom C. 1984. The gene order for rubella virus structural proteins is NH2-C-E2-E1-COOH. J. Virol. **51**:354–358.
13. Suomalainen M, Garoff H, Baron MD. 1990. The E2 signal sequence of rubella virus remains part of the capsid protein and confers membrane association *in vitro*. J. Virol. **64**:5500–5509.
14. Oker-Blom C, Ulmanen I, Kaariainen L, Pettersson RF. 1984. Rubella virus 40S genome RNA specifies a 24S subgenomic mRNA that codes for a precursor to structural proteins. J. Virol. **49**:403–408.
15. Tzeng WP, Frey TK. 2005. Rubella virus capsid protein modulation of viral genomic and subgenomic RNA synthesis. Virology **337**:327–334. http://dx.doi.org/10.1016/j.virol.2005.04.019.
16. Chen MH, Icenogle JP. 2004. Rubella virus capsid protein modulates viral genome replication and virus infectivity. J. Virol. **78**:4314–4322. http://dx.doi.org/10.1128/JVI.78.8.4314-4322.2004.
17. Tzeng WP, Matthews JD, Frey TK. 2006. Analysis of rubella virus capsid protein-mediated enhancement of replicon replication and mutant rescue. J. Virol. **80**:3966–3974. http://dx.doi.org/10.1128/JVI.80.8.3966-3974.2006.
18. Law LJ, Ilkow CS, Tzeng WP, Rawluk M, Stuart DT, Frey TK, Hobman TC. 2006. Analyses of phosphorylation events in the rubella virus capsid protein: role in early replication events. J. Virol. **80**:6917–6925. http://dx.doi.org/10.1128/JVI.01152-05.
19. Ilkow CS, Mancinelli V, Beatch MD, Hobman TC. 2008. Rubella virus capsid protein interacts with poly(A) -binding protein and inhibits translation. J. Virol. **82**:4284–4294. http://dx.doi.org/10.1128/JVI.02732-07.
20. Claus C, Chey S, Heinrich S, Reins M, Richardt B, Pinkert S, Fechner H, Gaunitz F, Schafer I, Seibel P, Liebert UG. 2011. Involvement of p32 and microtubules in alteration of mitochondrial functions by rubella virus. J. Virol. **85**:3881–3892. http://dx.doi.org/10.1128/JVI.02492-10.
21. Ilkow CS, Goping IS, Hobman TC. 2011. The rubella virus capsid is an anti-apoptotic protein that attenuates the pore-forming ability of Bax. PLoS Pathog. **7**:e1001291. http://dx.doi.org/10.1371/journal.ppat.1001291.
22. Kujala P, Ahola T, Ehsani N, Auvinen P, Vihinen H, Kaariainen L. 1999. Intracellular distribution of rubella virus nonstructural protein p150. J. Virol. **73**:7805–7811.
23. Garbutt M, Law LM, Chan H, Hobman TC. 1999. Role of rubella virus glycoprotein domains in assembly of virus-like particles. J. Virol. **73**:3524–3533.
24. Law LM, Duncan R, Esmaili A, Nakhasi HL, Hobman TC. 2001. Rubella virus E2 signal peptide is required for perinuclear localization of capsid protein and virus assembly. J. Virol. **75**:1978–1983. http://dx.doi.org/10.1128/JVI.75.4.1978-1983.2001.
25. Tellinghuisen TL, Hamburger AE, Fisher BR, Ostendorp R, Kuhn RJ. 1999. *In vitro* assembly of alphavirus cores by using nucleocapsid protein expressed in *Escherichia coli*. J. Virol. **73**:5309–5319.
26. Perera R, Owen KE, Tellinghuisen TL, Gorbalenya AE, Kuhn RJ. 2001. Alphavirus nucleocapsid protein contains a putative coiled coil alpha-helix important for core assembly. J. Virol. **75**:1–10. http://dx.doi.org/10.1128/JVI.75.1.1-10.2001.
27. Subba-Reddy CV, Goodfellow I, Kao CC. 2011. VPg-primed RNA synthesis of norovirus RNA-dependent RNA polymerases by using a novel cell-based assay. J. Virol. **85**:13027–13037. http://dx.doi.org/10.1128/JVI.06191-11.
28. Zuniga S, Sola I, Moreno JL, Sabella P, Plana-Duran J, Enjuanes L. 2007. Coronavirus nucleocapsid protein is an RNA chaperone. Virology **357**:215–227. http://dx.doi.org/10.1016/j.virol.2006.07.046.
29. Lulla V, Kim DY, Frolova EI, Frolov I. 2013. The amino-terminal domain of alphavirus capsid protein is dispensable for viral particle assembly but regulates RNA encapsidation through cooperative functions of its subdomains. J. Virol. **87**:12003–12019. http://dx.doi.org/10.1128/JVI.01960-13.
30. Reichert VL, Choi M, Petrillo JE, Gehrke L. 2007. Alfalfa mosaic virus coat protein bridges RNA and RNA-dependent RNA polymerase *in vitro*. Virology **364**:214–226. http://dx.doi.org/10.1016/j.virol.2007.02.026.
31. Zuniga S, Cruz JL, Sola I, Mateos-Gomez PA, Palacio L, Enjuanes L. 2010. Coronavirus nucleocapsid protein facilitates template switching and is required for efficient transcription. J. Virol. **84**:2169–2175. http://dx.doi.org/10.1128/JVI.02011-09.
32. Guogas LM, Laforest SM, Gehrke L. 2005. Coat protein activation of alfalfa mosaic virus replication is concentration dependent. J. Virol. **79**:5752–5761. http://dx.doi.org/10.1128/JVI.79.9.5752-5761.2005.
33. Liu J, Zheng Q, Deng Y, Cheng CS, Kallenbach NR, Lu M. 2006. A seven-helix coiled coil. Proc. Natl. Acad. Sci. U. S. A. **103**:15457–15462. http://dx.doi.org/10.1073/pnas.0604871103.
34. Parry DA, Fraser RD, Squire JM. 2008. Fifty years of coiled-coils and alpha-helical bundles: a close relationship between sequence and structure. J. Struct. Biol. **163**:258–269. http://dx.doi.org/10.1016/j.jsb.2008.01.016.
35. Communie G, Crepin T, Maurin D, Jensen MR, Blackledge M, Ruigrok RW. 2013. Structure of the tetramerization domain of measles virus phosphoprotein. J. Virol. **87**:7166–7169. http://dx.doi.org/10.1128/JVI.00487-13.
36. Tarbouriech N, Curran J, Ruigrok RW, Burmeister WP. 2000. Tetrameric coiled coil domain of Sendai virus phosphoprotein. Nat. Struct. Biol. **7**:777–781. http://dx.doi.org/10.1038/79013.
37. Bullough PA, Hughson FM, Skehel JJ, Wiley DC. 1994. Structure of influenza haemagglutinin at the pH of membrane fusion. Nature **371**:37–43. http://dx.doi.org/10.1038/371037a0.
38. Chan DC, Fass D, Berger JM, Kim PS. 1997. Core structure of gp41 from the HIV envelope glycoprotein. Cell **89**:263–273. http://dx.doi.org/10.1016/S0092-8674(00)80205-6.
39. Ma L, Jones CT, Groesch TD, Kuhn RJ, Post CB. 2004. Solution structure of dengue virus capsid protein reveals another fold. Proc. Natl. Acad. Sci. U. S. A. **101**:3414–3419. http://dx.doi.org/10.1073/pnas.0305892101.
40. Mangala Prasad V, Willows SD, Fokine A, Battisti AJ, Sun S, Plevka P, Hobman TC, Rossmann MG. 2013. Rubella virus capsid protein structure and its role in virus assembly and infection. Proc. Natl. Acad. Sci. U. S. A. **110**:20105–20110. http://dx.doi.org/10.1073/pnas.1316681110.
41. Lee JY, Hwang D, Gillam S. 1996. Dimerization of rubella virus capsid protein is not required for virus particle formation. Virology **216**:223–227. http://dx.doi.org/10.1006/viro.1996.0051.
42. Hale BG, Kerry PS, Jackson D, Precious BL, Gray A, Killip MJ, Randall RE, Russell RJ. 2010. Structural insights into phosphoinositide 3-kinase activation by the influenza A virus NS1 protein. Proc. Natl. Acad. Sci. U. S. A. **107**:1954–1959. http://dx.doi.org/10.1073/pnas.0910715107.
43. Zhang Y, Chan NC, Ngo HB, Gristick H, Chan DC. 2012. Crystal structure of mitochondrial fission complex reveals scaffolding function for mitochondrial division 1 (Mdv1) coiled coil. J. Biol. Chem. **287**:9855–9861. http://dx.doi.org/10.1074/jbc.M111.329359.
44. Tzeng WP, Frey TK. 2003. Complementation of a deletion in the rubella virus p150 nonstructural protein by the viral capsid protein. J. Virol. **77**:9502–9510. http://dx.doi.org/10.1128/JVI.77.17.9502-9510.2003.
45. Tzeng WP, Frey TK. 2009. Functional replacement of a domain in the rubella virus p150 replicase protein by the virus capsid protein. J. Virol. **83**:3549–3555. http://dx.doi.org/10.1128/JVI.02411-08.
46. Claus C, Tzeng WP, Liebert UG, Frey TK. 2012. Rubella virus-like replicon particles: analysis of encapsidation determinants and nonstructural roles of capsid protein in early post-entry replication. J. Gen. Virol. **93**:516–525. http://dx.doi.org/10.1099/vir.0.038984-0.
47. Matthews JD, Tzeng WP, Frey TK. 2012. Determinants in the maturation of rubella virus p200 replicase polyprotein precursor. J. Virol. **86**:6457–6469. http://dx.doi.org/10.1128/JVI.06132-11.
48. Liu Z, Yang D, Qiu Z, Lim KT, Chong P, Gillam S. 1996. Identification of domains in rubella virus genomic RNA and capsid protein necessary for specific interaction. J. Virol. **70**:2184–2190.
49. Perera R, Navaratnarajah C, Kuhn RJ. 2003. A heterologous coiled coil can substitute for helix I of the Sindbis virus capsid protein. J. Virol. **77**:8345–8353. http://dx.doi.org/10.1128/JVI.77.15.8345-8353.2003.
50. Owen KE, Kuhn RJ. 1996. Identification of a region in the Sindbis virus nucleocapsid protein that is involved in specificity of RNA encapsidation. J. Virol. **70**:2757–2763.
51. Tellinghuisen TL, Kuhn RJ. 2000. Nucleic acid-dependent cross-linking of the nucleocapsid protein of Sindbis virus. J. Virol. **74**:4302–4309. http://dx.doi.org/10.1128/JVI.74.9.4302-4309.2000.
52. Tellinghuisen TL, Perera R, Kuhn RJ. 2001. *In vitro* assembly of Sindbis virus core-like particles from cross-linked dimers of truncated and mutant capsid proteins. J. Virol. **75**:2810–2817. http://dx.doi.org/10.1128/JVI.75.6.2810-2817.2001.
53. Hong EM, Perera R, Kuhn RJ. 2006. Alphavirus capsid protein helix I controls a checkpoint in nucleocapsid core assembly. J. Virol. **80**:8848–8855. http://dx.doi.org/10.1128/JVI.00619-06.
54. Hobman TC, Lundstrom ML, Mauracher CA, Woodward L, Gillam S, Farquhar MG. 1994. Assembly of rubella virus structural proteins into

virus-like particles in transfected cells. Virology 202:574–585. http://dx.doi.org/10.1006/viro.1994.1379.
55. Sakata M, Komase K, Nakayama T. 2009. Histidine at position 1042 of the p150 region of a KRT live attenuated rubella vaccine strain is responsible for the temperature sensitivity. Vaccine 27:234–242. http://dx.doi.org/10.1016/j.vaccine.2008.10.049.
56. Sakata M, Nakayama T. 2011. Protease and helicase domains are related to the temperature sensitivity of wild-type rubella viruses. Vaccine 29:1107–1113. http://dx.doi.org/10.1016/j.vaccine.2010.11.074.
57. Virnik K, Ni Y, Berkower I. 2012. Live attenuated rubella viral vectors stably express HIV and SIV vaccine antigens while reaching high titers. Vaccine 30:5453–5458. http://dx.doi.org/10.1016/j.vaccine.2012.06.074.

Journal of Virological Methods 207 (2014) 73–77

Contents lists available at ScienceDirect

Journal of Virological Methods

journal homepage: www.elsevier.com/locate/jviromet

Short communication

Development of an improved RT-LAMP assay for detection of currently circulating rubella viruses

H. Abo[a], K. Okamoto[a,*], M. Anraku[a], N. Otsuki[a], M. Sakata[a], J. Icenogle[b], Q. Zheng[b], T. Kurata[c], T. Kase[c], K. Komase[a], M. Takeda[a], Y. Mori[a]

[a] Laboratory of Rubella, Department of Virology III, National Institute of Infectious Diseases, Murayama Branch, 4-7-1 Gakuen, Musashimurayama, 208-0011, Tokyo, Japan
[b] Measles, Mumps, Rubella and Herpes Virus Laboratory Branch, Division of Viral Diseases, Centers for Disease Control and Prevention, 1600 Clifton Road, Atlanta, GA 30333, USA
[c] Virology Division, Department of Infectious Diseases, Osaka Prefectural Institute of Public Health, 3-69, Nakamichi, 1-chome, Higashinari-ku, Osaka 537-0025, Japan

Article history:
Received 31 March 2014
Received in revised form 12 June 2014
Accepted 17 June 2014
Available online 24 June 2014

Keywords:
Rubella
Diagnosis
RT-LAMP

ABSTRACT

Rubella virus is the causative agent of rubella. The symptoms are usually mild, and characterized by a maculopapular rash and fever. However, rubella infection in pregnant women sometimes can result in the birth of infants with congenital rubella syndrome (CRS). Global efforts have been made to reduce and eliminate CRS. Although a reverse transcription-loop-mediated isothermal amplification (RT-LAMP) assay for detection of rubella virus has been reported, the primers contained several mismatched nucleotides with the genomes of currently circulating rubella virus strains. In the present study, a new RT-LAMP assay was established. The detection limit of this assay was 100–1000 PFU/reaction of viruses for all rubella genotypes, except for genotype 2C, which is not commonly found in the current era. Therefore, the new RT-LAMP assay can successfully detect all current rubella virus genotypes, and does not require sophisticated devices like TaqMan real-time PCR systems. This assay should be a useful assay for laboratory diagnosis of rubella and CRS.

© 2014 Elsevier B.V. All rights reserved.

Rubella virus (RV) is the causative agent of rubella, also known as German measles. RV is the sole member of the genus *Rubivirus* in the family Togaviridae and its genome consists of a single positive-strand RNA of approximately 9.8 kb in length. The viral genome contains two open reading frames (ORFs). The 5′ ORF encodes two non-structural proteins (p150 and p90) (Pugachev et al., 1997; Liang and Gillam, 2000) and the 3′ ORF encodes three structural proteins (E1, E2 and C) (Oker-Blom et al., 1984; Frey, 1994; Yao et al., 1998). Although RV has only one serotype, 13 genotypes have been reported to date, based on analyses of the structural protein gene nucleotide sequences (Abernathy et al., 2011; WHO, 2013). The 13 genotypes are classified into two clades, clade 1 and clade 2. Clade 1 consists of genotypes 1a, 1B, 1C, 1D, 1E, 1F, 1G, 1H, 1I, and 1J, while clade 2 consists of genotypes 2A, 2B, and 2C (WHO, 2013). Genotypes 1E, 1G, 1H, 1J, and 2B were the major RV genotypes circulating worldwide between 2005 and 2010 (Abernathy et al., 2011). Among these, genotypes 1E, 1J, and 2B constitute the majority of RV isolates in East and South-East Asia.

The typical symptoms of rubella are relatively mild, and characterized by a maculopapular rash, short-duration fever, and lymphadenopathy. RV infection of women within the first trimester of pregnancy can cause miscarriage, fetal death, or birth of infants with congenital rubella syndrome (CRS), which includes various birth defects such as sensorineural deafness, heart defects, and cataracts. Rubella is effectively prevented by vaccination with rubella-containing vaccines. In the last two decades, the number of member states of the World Health Organization (WHO) that have introduced rubella-containing vaccines into their national immunization schedules has increased significantly (from 83 in 1996 to 130 in 2009) (WHO, 2011). The WHO Region of the Americas (AMR or PAHO) and European Region (EUR) have established goals to eliminate rubella by 2010 and 2015, respectively. PAHO is verifying rubella and CRS elimination at present. However, in many countries, especially developing countries, RCVs have not yet been introduced and rubella and CRS surveillance has been weak. Thus, a significant number of CRS cases are likely overlooked in these countries (WHO, 2011).

* Corresponding author. Tel.: +81 42 561 0771; fax: +81 42 561 1960.
E-mail address: k-okmt@nih.go.jp (K. Okamoto).

http://dx.doi.org/10.1016/j.jviromet.2014.06.013
0166-0934/© 2014 Elsevier B.V. All rights reserved.

Table 1
Primers used for the RT-LAMP assay.

	Primers	Genomic positions	Sequence (5′-3′)
NSP	FIP_NSP5	(251–230)+(171–187)	cgtggagtgctgggtgatcactcccaRaagcgggccatc
	BIP_NSP5	(257–274)+(324–306)	tcgcggtatacccgccgcggggtcgatSaggacgtgta
	F3_NSP5	97–115	cggcagttgggtaagagac
	B3_NSP5	395–380	ccgtcctgtggaggca
	Loop F_NSP5	218–196	gcgtgaaHacaggtctgggtatc
	Loop B_NSP5	286–304	gtggggccctaaagaagcc
E1	FIP_E1	(8557–8539)+(8495–8510)	agaggccagctgcgcgtaccgcgcgtgcaccttct
	BIP_E1	(8600–8617)+(8666–8651)	accgcgtgcgaggttgaatgtcggtggggaagcc
	F3_E1	8475–8494	gcatctggaatggcacacag
	B3_E1	8686–8669	ccgcttgtgcgagtagtg
	Loop F_E1	8535–8521	ccagaggagtaggcg
	Loop B_E1	8618–8632	cctgccttcggacac

Since clinical diagnosis of rubella and CRS is often unreliable, laboratory confirmation is critical. The WHO recommends testing for anti-rubella IgM in serum as the standard method for laboratory diagnosis of rubella. However, anti-rubella IgM may be undetectable until a few days after rash and fever appearance (CDC, 2008; WHO, 2008). On the other hand, viral genome detection can be used to confirm rubella in the first few days after rash appearance, since virus is excreted about 1 week before the rash appearance and the peak of its excretion in the oral fluid coincides with rash appearance. Viral genome detection can also be used to confirm CRS (Bellini and Icenogle, 2011). Several methods, including RT-PCR (or RT-nested PCR) (Zhu et al., 2007), real-time RT-PCR (Okamoto et al., 2010), and RT-loop-mediated isothermal amplification (RT-LAMP) (Mori et al., 2006), have been established for detection of the RV genome.

LAMP was developed for amplification of target DNA with a specific primer set and a DNA polymerase with strand displacement activity (Notomi et al., 2000; Nagamine et al., 2002). LAMP has high specificity because at least four specific primers corresponding to six regions are required for the amplification (Notomi et al., 2000; Nagamine et al., 2002). The LAMP reaction is usually carried out under isothermal conditions at about 65 °C for about 1 h. Therefore, the laboratory diagnosis is easily conducted using simple devices. Importantly, the results can be assessed visually without opening of the sample tubes, which decreases the risk of cross-contamination. There are several methods for detection of LAMP amplification products. Turbidity derived from precipitated magnesium pyrophosphate as a by-product of the amplification is generally employed for LAMP detection (Mori et al., 2001). Turbidity can be monitored in real-time using a turbidimeter or detected visually. Detection by color change after addition of hydroxyl naphthol blue (HNB) to the reaction mixture has also been reported (Goto et al., 2009). HNB is a colorimetric reagent for alkaline earth metal ions. The concentration of magnesium ions in the LAMP reaction mixture decreases during amplification. If amplification occurs, the solution including HNB changes from violet to sky-blue. Users can select a detection method according to their situation. An RNA template can also be amplified by LAMP, by combination with a reverse transcription reaction (RT-LAMP) (Notomi et al., 2000). RT-LAMP has been adapted to detect RNA virus infections (Ushio et al., 2005; Ito et al., 2006). Mori et al. (2006) reported previously an RT-LAMP assay for the RV genome using primers targeting the nucleotide sequence of the E1 region, which were designed based on the KRT vaccine strain (genotype 1a) genome sequence. However, the E1 region is variable in its nucleotide sequences, and the original primers display some mismatches with several RV genotypes, especially 1J, 1E, and 2B, the major genotypes recently circulating in Japan (data not shown). This suggests that the RT-LAMP assay using these mismatched primers may show low sensitivity for detection of these RV genotypes. In the present study, to refine the RT-LAMP assay for detection of currently circulating RV genotypes, we designed new primers targeting the 5′-terminal region of the non-structural protein gene encoding p150. The targeted region is adjacent to the primer-targeted region in a TaqMan real-time PCR method reported previously (Okamoto et al., 2010). The performance of the new RT-LAMP assay developed in this study was examined using viral RNAs of all genotypes.

The new RT-LAMP primer set, named the NSP primer set, was designed using an online software program for LAMP primer design (PrimerExplorer; http://primerexplorer.jp/index.html) to target the region of nucleotides 97–395, a highly conserved region among various genotypes. The primer sequences and positions are shown in Table 1. Previously described primers are also shown in Table 1. The RT-LAMP assay was performed using a Loopamp RNA amplification kit (RT-LAMP; EIKEN Chemical, Tokyo, Japan). An aliquot (5 μl) of each RNA was mixed with 40 pmol of FIP and BIP primers, 20 pmol of Loop-F and Loop-B primers, 5 pmol of F3 and B3 primers, 1 μl of enzyme mix, and 12.5 μl of reaction mix in a total volume of 25 μl. The reaction mixture was incubated at 63 °C for 60 min followed by 85 °C for 5 min in a Loopamp real-time turbidimeter (RT-160C; EIKEN Chemical). The assay was performed in triplicate for each sample, and a no-template control, in which the RNA template was omitted, was included in each assay. Test samples were considered positive if the turbidity signal was greater than 0.1 after 60 min. Controls without template gave no turbidity signals typically, by both a measuring device and visually. A 10-fold dilution series of *in vitro* synthesized RNA (nucleotides 1–782 of the TO-336 strain) was prepared as the standard RNAs (from 2.0×10^5 to 2.0×10^{-1} copies/μl) as described previously (Okamoto et al., 2010). Three distinct sets of standard RNA samples (1.0×10^6 to 1 copies/reaction) were prepared totally independently (starting with *in vitro* transcriptions from plasmids) examined to estimate the detection limit of the assay. Although $>10^4$ copies/reaction were detected in all samples, 10^3 copies/reaction were detected in 78% of samples (Table 2). The

Table 2
Detection limit of the RT-LAMP assay using a series of synthesized standard RNA solutions.

Standard RNA (copies/reaction)	Number of positive samples/number of tested samples			Positive (%)
	1	2	3	
10^6	3/3	3/3	3/3	100
10^5	3/3	3/3	3/3	100
10^4	3/3	3/3	3/3	100
10^3	2/3	2/3	3/3	78
10^2	0/3	0/3	1/3	11
10	0/3	0/3	0/3	0
50% detection dose*	2.75	2.75	2.25	2.58**

* Copies of standard RNA for which 50% of reactions were positive ($\log_{10}$ copies/ml).
** Mean value of three trials.

Table 3
Sensitivity of the RT-PCR assay for different genotypes: test results (P* or N**) with the time (minutes) when turbidity signals passed the cutoff.

Strain		Viral dose (PFU)			
	10^3	10^2	10^1	10^0	
RVi/BEL/63[1a]VAC	1a	P (25.6 ± 5.21)***	P (30.5 ± 3.80)	N (>60.0)	N (>60.0)
RVi/Jerusalem.ISR/75[1B]	1B	P (20.7 ± 3.56)	N (>60.0)	N (>60.0)	N (>60.0)
RVi/Los Angels.USA/91[1 C]	1C	P (22.6 ± 2.52)	P (32.0 ± 2.08)	N (>60.0)	N (>60.0)
Osaka '94	1D	P (24.1 ± 5.21)	N (>60.0)	N (>60.0)	N (>60.0)
Rvi/Dezhou.CHN/02[1E]	1E	P (20.4 ± 2.70)	P (27.4 ± 3.66)	N (>60.0)	N (>60.0)
Rvi/Linqing.CHN/00[1F]	1F	P (23.0 ± 3.07)	N (>60.0)	N (>60.0)	N (>60.0)
Rvi/UGA/20.01[1G]	1G	P (18.4 ± 0.97)	P (25.4 ± 2.87)	N (>60.0)	N (>60.0)
Rvi/Minsk.BLR/28.05[1H]	1H	P (19.7 ± 0.62)	P (26.1 ± 1.03)	N (>60.0)	N (>60.0)
Rvi/Milan.ITA/46.92[1I]	1I	P (22.9 ± 2.81)	P (31.2 ± 6.42)	N (>60.0)	N (>60.0)
Rvi/Miyazaki.JPN/10.01 CRS[1J]	1J	P (21.7 ± 1.87)	N (>60.0)	N (>60.0)	N (>60.0)
Rvi/Beijing.CHN/80[2A]VAC	2A	P (22.5 ± 2.39)	P (31.1 ± 2.34)	N (>60.0)	N (>60.0)
Rvi/Telaviv.ISR/68[2B]	2B	P (24.8 ± 4.41)	N(>60.0)	N (>60.0)	N (>60.0)
Rvi/Moscow.RUS/67[2 C]	2C	N (>60.0)	N (>60.0)	N (>60.0)	N (>60.0)

* P: positive.
** N: negative.
*** Data represent the mean values calculated from three independent experiments.

end-point, at which 50% of the reactions were positive, was calculated by the Reed-Müench method (Reed and Muench, 1938), and was about 380 copies/reaction. This detection limit was higher than that of the TaqMan real-time PCR assay, which could detect all samples at 10 copies/reaction (Okamoto et al., 2010). The sensitivities of the TaqMan and RT-LAMP assays were reported to be similar for detection of Chikungunya virus and Rift Valley virus (Le Roux et al., 2009; Reddy et al., 2012). The sensitivity of the RT-LAMP assay may be lower than that of the TaqMan real-time PCR assay Because of a complicated secondary structure. The RV genome may form a complicated secondary structure owing to its high (~70%) GC contents (Frey, 1994). Next, we examined whether the new RT-LAMP assay could detect the genomes of all 13 RV genotypes. The 13 RVs were propagated with Vero cells or RK-13 cells. The viral RNA was extracted from 140 μl aliquots of serial dilutions of these virus samples using a QIAamp Viral RNA Mini Kit (QIAGEN, Tokyo, Japan) according to the manufacturer's protocol. To assess the sensitivity of the RT-LAMP (NSP primer set) assay for different genotypes, 5 μl of each RNA extract of the 13 RVs was amplified with the assay (Table 3). Some examples of the time course of turbidity measured by a Loopamp real-time turbidimeter were cited in Fig. 1. Test samples were considered positive if amplification was seen in all triplicate reactions, and three independent experiments were repeated. Table 3

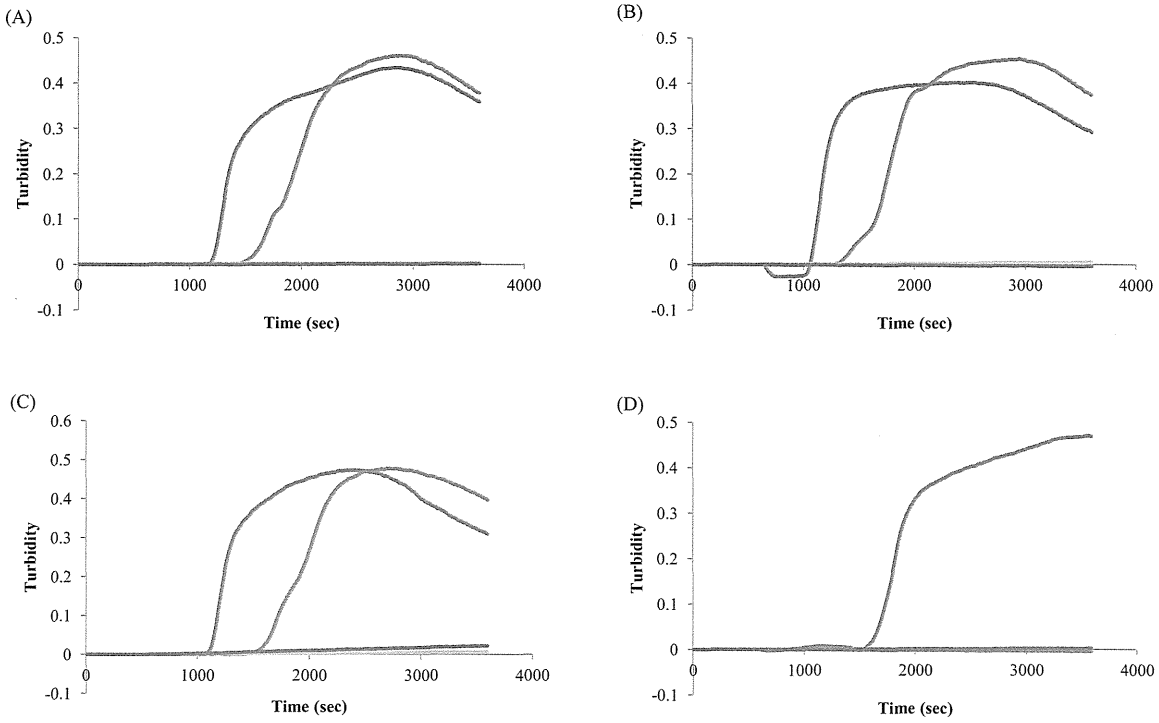

Fig. 1. The time course of turbidity by RT-LAMP assay. The graphs showed the turbidity measured by a Loopamp real-time turbidimeter. Blue, red, green, and violet lines represent 10^3, 10^2, 10, and 1 PFU/reaction of virus strains as follows, respectively. (A) Rvi/Dezhou.CHN/02[1E]; (B) Rvi/Minsk.BLR/28.05[1H]; (C) Rvi/Miyazaki.JPN/10.01 CRS[1J]; (D) Rvi/Telaviv.ISR/68[2B].

Table 4
Sensivity comparisons of the primer sets: test results (P* or N**) with the time (minutes) when turbidity signals passed the cutoff.

Strain		Viral dose (PFU)							
		10^3		10^2		10^1		10^0	
	NSP***	E1*	NSP	E1	NSP	E1	NSP	E1	
Rvi/Dezhou.CHN/02	1E	P (19.25 ± 0.52)****	P (23.81 ± 1.39)	P (27.68 ± 1.62)	P (27.92 ± 2.15)	N (>60.0)	N (>60.0)	N (>60.0)	N (>60.0)
Rvi/Minsk.BLR/28.05	1H	P (18.33 ± 1.40)	P (24.17 ± 1.68)	P (24.01 ± 3.67)	P (27.82 ± 2.71)	N (>60.0)	N (>60.0)	N (>60.0)	N (>60.0)
Rvi/Miyazaki.JPN/10.01 CRS	1J	P (18.04 ± 0.64)	P (28.81 ± 2.02)	P (24.28 ± 3.97)	P (36.08 ± 5.24)	N (>60.0)	N (>60.0)	N (>60.0)	N (>60.0)
Rvi/Telaviv.ISR/68	2B	P (22.08 ± 2.25)	N (>60.0)	N (>60.0)	N (>60.0)	N (>60.0)	N (>60.0)	N (>60.0)	N (>60.0)

* P: positive.
** N: negative.
*** NSP and E1 are the primer sets used in this study and previously reported, respectively.
**** Data represent the mean values calculated from three independent experiments.

shows the average values, as the times (in minutes) when the turbidity signal was beyond the threshold. The data indicated that 100–1000 PFU/reaction of virus was required for detection by the new RT-LAMP assay, except for the genotype 2C virus (RVi/Moscow.RUS/67).

The assay failed to detect the genotype 2C virus, whereas the TaqMan real-time PCR assay could detect 10 PFU/reaction of this virus (data not shown). The geographical location of genotype 2C viruses was restricted to Russia, and genotype 2C viruses have not been detected since 2005. Thus, the problem in detecting genotype 2C viruses is likely not an important obstacle for the new RT-LAMP assay. However, this problem may require consideration when using the assay.

It is necessary to distinguish rubella from measles that has the similar clinical symptoms with rubella. The specificity of the new RT-LAMP assay was tested using measles virus RNA derived from genotype D3, D5, D8, and H1. No amplification was found with the RT-LAMP assay even with about 6 $\log_{10}$ copies/reaction, thus the RT-LAMP assay was thought not to cross-react with measles virus genomes (data not shown).

The sensitivity of the new NSP primer set was compared with the primer set reported previously by Mori et al. (2006). The primer set used by Mori et al. was targeted to the E1 structural protein gene (Table 1), and was thus designated the "E1 primer set" in this study. RNA extracts from virus stocks of four major genotypes circulating in the world were subjected to the RT-LAMP assay using either the NSP primer set or E1 primer set (Table 4). Both assays detected 100 PFU of RV genotypes 1E (Rvi/Dezhou.CHN/02), 1h (Rvi/Minsk.BLR/28.05), and 1J (Rvi/Miyazaki.JPN/10.01 CRS), suggesting that for RV genotypes 1E, 1H, and 1J, the sensitivity of the assay targeting the non-structural protein gene was comparable to that targeting the E1 gene reported by Mori et al. (2006). On the other hand, the E1 primer set failed to detect the genotype 2B RV (Rvi/Telaviv.ISR/68), while the NSP primer set detected it successfully, suggesting that the NSP primer set was useful for detection of 2B genotype viruses. Mori et al. (2006) described that the detection limit of their assay was approximately 1 PFU of virus. The difference in the detection limits between the assays may arise from differences in determination of the detection limits by PFU. Specifically, diluted viral RNA serially after extraction from virus stock was used previously while we used viral RNA extracted from serially diluted virus stocks to more closely resemble actual specimens with low amount of virus. The E1 primer set exhibited an almost equivalent detection limit to the NSP primer set under the conditions used in this study (Table 4). Finally, a spike test was performed using a similar procedure to previously reported method (Okamoto et al., 2010). Briefly, four viral strain stocks, Rvi/Dezhou.CHN/02[1E], Rvi/Minsk.BLR/28.05[1h], Rvi/Telaviv.ISR/68[2B], and Rvi/Miyazaki.JPN/10.01 CRS[1j], were diluted to 10^5, 10^4, 10^3, 10^2, and 10^1 PFU/ml with throat swabs from healthy donors collected in Universal Viral Transport Medium (BD, Franklin Lakes, NJ), and viral RNAs were extracted from 140 μl aliquots of these samples. Five microliters of each viral RNA extract was subjected to the RT-LAMP assay using the NSP primer set (Table 5). For all of the tested genotypes, the spike test showed similar sensitivity to that using viral RNA extracted from culture medium (Tables 4 and 5). Therefore, neither the RNA extraction steps nor the amplification steps of the RT-LAMP assay were affected by the presence of RNAs typically found in normal throat swabs.

In this study, the RT-LAMP assay was improved for detection of RV strains currently circulating in the world. The improved assay detected successfully RV genotypes 1E, 1H, 1J, and 2B, the current major genotypes worldwide. Therefore, the improved RT-LAMP assay should be a useful assay for laboratory diagnosis of rubella. The assay is less sensitive than some real-time assays, a fact which should be considered when dealing with samples containing small amount of RV RNA. However, the RT-LAMP assay can be used for rapid laboratory diagnosis, does not require sophisticated devices like real-time PCR systems, and decreases the risk of laboratory contamination because of the lack of handling procedures for the amplified products. Surveillance for rubella and CRS using RNA detection for laboratory confirmation is problematic in many countries; the improved assay described here could improve RNA confirmation in these countries.

Table 5
Spike tests: test results (P* or N**) with the time (minutes) when turbidity signals passed the cutoff.

Strain		Viral dose (PFU)			
	10^3	10^2	10^1	10^0	
Rvi/Dezhou.CHN/02	1E	P (22.74 ± 4.38)***	P (29.78 ± 4.01)	N (>60.0)	N (>60.0)
Rvi/Minsk.BLR/28.05	1H	P (20.12 ± 1.39)	P (26.24 ± 2.57)	N (>60.0)	N (>60.0)
Rvi/Telaviv.ISR/68	2B	P (22.30 ± 0.30)	N (>60.0)	N (>60.0)	N (>60.0)
Rvi/Miyazaki.JPN/10.01 CRS	1J	P (25.36 ± 4.90)	N (>60.0)	N (>60.0)	N (>60.0)

* P: positive.
** N: negative.
*** Data represent the mean values calculated from three independent experiments.

Disclaimer

The findings and conclusions in this report are those of the author(s) and do not necessarily represent the official position of the Centers for Disease Control and Prevention.

Acknowledgements

This work was supported by Grants-in-Aid from the Ministry of Health, Labour and Welfare, Science Research Grant(s) (H24-Iyaku-Ippan-008 and H25-Shinko-Ippan-010). We thank Dr. P. Rota and all members of Measles, Mumps, Rubella and Herpes Virus Laboratory Branch, Division of Viral Diseases, Centers for Disease Control and Prevention, for their helpful discussions.

References

Abernathy, E.S., Hübschen, J.M., Muller, C.P., Jin, L., Brown, D., Komase, K., Mori, Y., Xu, W., Zhu, Z., Siqueira, M.M., Shulga, S., Tikhonova, N., Pattamadilok, S., Incomserb, P., Smit, S.B., Akoua-Koffi, C., Bwogi, J., Lim, W.W., Woo, G.K., Triki, H., Jee, Y., Mulders, M.N., de Filippis, A.M., Ahmed, H., Ramamurty, N., Featherstone, D., Icenogle, J.P., 2011. Status of global virologic surveillance for rubella viruses. J. Infect. Dis. 204 (Suppl. 1), S524–S532.

Bellini, B., Icenogle, J., 2011. Measles and rubella. Man. Clin. Microbiol. 2, 1378–1387.

CDC, 2008. Recommendations from an ad hoc Meeting of the WHO Measles and Rubella Laboratory Network (LabNet) on use of alternative diagnostic samples for measles and rubella surveillance. Morb. Mortal. Wkly. Rep. 57, 657–660.

Frey, T.K., 1994. Molecular biology of rubella virus. Adv. Virus Res. 44, 69–160.

Goto, M., Honda, E., Ogura, A., Nomoto, A., Hanaki, K., 2009. Colorimetric detection of loop-mediated isothermal amplification reaction by using hydroxy naphthol blue. Biotechniques 46, 167–172.

Ito, M., Watanabe, M., Nakagawa, N., Ihara, T., Okuno, Y., 2006. Rapid detection and typing of influenza A and B by loop-mediated isothermal amplification: comparison with immunochromatography and virus isolation. J. Virol. Methods 135, 272–275.

Le Roux, C.A., Kubo, T., Grobbelaar, A.A., van Vuren, P.J., Weyer, J., Nel, L.H., Swanepoel, R., Morita, K., Paweska, J.T., 2009. Development and evaluation of a real-time reverse transcription-loop-mediated isothermal amplification assay for rapid detection of Rift Valley fever virus in clinical specimens. J. Clin. Microbiol. 47, 645–651.

Liang, Y., Gillam, S., 2000. Mutational analysis of the rubella virus nonstructural polyprotein and its cleavage products in virus replication and RNA synthesis. J. Virol. 74, 5133–5141.

Mori, Y., Nagamine, K., Tomita, N., Notomi, T., 2001. Detection of loop-mediated isothermal amplification reaction by turbidity derived from magnesium pyrophosphate formation. Biochem. Biophys. Res. Commun. 289, 150–154.

Mori, N., Motegi, Y., Shimamura, Y., Ezaki, T., Natsumeda, T., Yonekawa, T., Ota, Y., Notomi, T., Nakayama, T., 2006. Development of a new method for diagnosis of rubella virus infection by reverse transcription-loop-mediated isothermal amplification. J. Clin. Microbiol. 44, 3268–3273.

Nagamine, K., Hase, T., Notomi, T., 2002. Accelerated reaction by loop-mediated isothermal amplification using loop primers. Mol. Cell. Probes 16, 223–229.

Notomi, T., Okayama, H., Masubuchi, H., Yonekawa, T., Watanabe, K., Amino, N., Hase, T., 2000. Loop-mediated isothermal amplification of DNA. Nucleic Acids Res. 28, E63.

Okamoto, K., Fujii, K., Komase, K., 2010. Development of a novel TaqMan real-time PCR assay for detecting rubella virus RNA. J. Virol. Methods 168, 267–271.

Oker-Blom, C., Ulmanen, I., Kääriäinen, L., Pettersson, R.F., 1984. Rubella virus 40S genome RNA specifies a 24S subgenomic mRNA that codes for a precursor to structural proteins. J. Virol. 49, 403–408.

Pugachev, K., Abernathy, E., Frey, T., 1997. Improvement of the specific infectivity of the rubella virus (RUB) infectious clone: determinants of cytopathogenicity induced by RUB map to the nonstructural proteins. J. Virol. 71, 562–568.

Reddy, V., Ravi, V., Desai, A., Parida, M., Powers, A.M., Johnson, B.W., 2012. Utility of IgM ELISA, TaqMan real-time PCR, reverse transcription PCR, and RT-LAMP assay for the diagnosis of Chikungunya fever. J. Med. Virol. 84, 1771–1778.

Reed, L.J., Muench, H., 1938. A simple method of estimating fifty percent endpoints. Am. J. Hyg. 27, 493–497.

Ushio, M., Yui, I., Yoshida, N., Fujino, M., Yonekawa, T., Ota, Y., Notomi, T., Nakayama, T., 2005. Detection of respiratory syncytial virus genome by subgroups-A, B specific reverse transcription loop-mediated isothermal amplification (RT-LAMP). J. Med. Virol. 77, 121–127.

WHO, 2008. Measles and rubella laboratory network: 2007 meeting on use of alternative sampling techniques for surveillance. Wkly. Epidemiol. Rec. 83, 225–232.

WHO, 2011. Rubella vaccines: WHO position paper. Wkly. Epidemiol. Rec. 86, 301–316.

WHO, 2013. Rubella virus nomenclature update. Wkly. Epidemiol. Rec. 88 (32), 337–343.

Yao, J., Yang, D., Chong, P., Hwang, D., Liang, Y., Gillam, S., 1998. Proteolytic processing of rubella virus nonstructural proteins. Virology 246, 74–82.

Zhu, Z., Xu, W., Abernathy, E.S., Chen, M., Zheng, Q., Wang, T., Zhang, Z., Li, C., Wang, C., He, W., Zhou, S., Icenogle, J., 2007. Comparison of four methods for confirming rubella virus infection using throat swabs. J. Clin. Microbiol., 452847–452852.

JVI
Journals.ASM.org

Epitope Mapping of the Hemagglutinin Molecule of A/(H1N1)pdm09 Influenza Virus by Using Monoclonal Antibody Escape Mutants

Yoko Matsuzaki,[a] Kanetsu Sugawara,[a] Mina Nakauchi,[b] Yoshimasa Takahashi,[c] Taishi Onodera,[c] Yasuko Tsunetsugu-Yokota,[c*] Takayuki Matsumura,[c] Manabu Ato,[c] Kazuo Kobayashi,[c*] Yoshitaka Shimotai,[a] Katsumi Mizuta,[d] Seiji Hongo,[a] Masato Tashiro,[b] Eri Nobusawa[b]

Department of Infectious Diseases, Yamagata University Faculty of Medicine, Yamagata, Japan[a]; Influenza Virus Research Center, National Institute of Infectious Diseases, Tokyo, Japan[b]; Department of Immunology, National Institute of Infectious Diseases, Tokyo, Japan[c]; Department of Microbiology, Yamagata Prefectural Institute of Public Health, Yamagata, Japan[d]

ABSTRACT

We determined the antigenic structure of pandemic influenza A(H1N1)pdm09 virus hemagglutinin (HA) using 599 escape mutants that were selected using 16 anti-HA monoclonal antibodies (MAbs) against A/Narita/1/2009. The sequencing of mutant HA genes revealed 43 amino acid substitutions at 24 positions in three antigenic sites, Sa, Sb, and Ca2, which were previously mapped onto A/Puerto Rico/8/34 (A/PR/8/34) HA (A. J. Caton, G. G. Brownlee, J. W. Yewdell, and W. Gerhard, Cell 31:417–427, 1982), and an undesignated site, i.e., amino acid residues 141, 142, 143, 171, 172, 174, 177, and 180 in the Sa site, residues 170, 173, 202, 206, 210, 211, and 212 in the Sb site, residues 151, 154, 156, 157, 158, 159, 200, and 238 in the Ca2 site, and residue 147 in the undesignated site (numbering begins at the first methionine). Sixteen MAbs were classified into four groups based on their cross-reactivity with the panel of escape mutants in the hemagglutination inhibition test. Among them, six MAbs targeting the Sa and Sb sites recognized both residues at positions 172 and 173. MAb n2 lost reactivity when mutations were introduced at positions 147, 159 (site Ca2), 170 (site Sb), and 172 (site Sa). We designated the site consisting of these residues as site Pa. From 2009 to 2013, no antigenic drift was detected for the A(H1N1)pdm09 viruses. However, if a novel variant carrying a mutation at a position involved in the epitopes of several MAbs, such as 172, appeared, such a virus would have the advantage of becoming a drift strain.

IMPORTANCE

The first influenza pandemic of the 21st century occurred in 2009 with the emergence of a novel virus originating with swine influenza, A(H1N1)pdm09. Although HA of A(H1N1)pdm09 has a common origin (1918 H1N1) with seasonal H1N1, the antigenic divergence of HA between the seasonal H1N1 and A(H1N1)pdm09 viruses gave rise to the influenza pandemic in 2009. To take precautions against the antigenic drift of the A(H1N1)pdm09 virus in the near future, it is important to identify its precise antigenic structure. To obtain various mutants that are not neutralized by MAbs, it is important to neutralize several plaque-cloned parent viruses rather than only a single parent virus. We characterized 599 escape mutants that were obtained by neutralizing four parent viruses of A(H1N1)pdm09 in the presence of 16 MAbs. Consequently, we were able to determine the details of the antigenic structure of HA, including a novel epitope.

The first influenza pandemic of the 21st century occurred in 2009. The pandemic strain, a novel swine-derived, triple reassortant A(H1N1)pdm09 (pdm09) virus, contained hemagglutinin (HA) that genetically originated with the 1918 Spanish influenza virus (1). Although the pdm09 virus was predominant in the world in the 2009/2010 and 2010/2011 influenza seasons, the A(H3N2) virus became predominant during the 2011/2012 and 2012/2013 seasons (2, 3) (see also the "Influenza virus activity in the world" website [http://www.who.int/influenza/gisrs_laboratory/updates/summaryreport_20120706/en/] and the "FluNet Summary" website [http://www.who.int/influenza/gisrs_laboratory/updates/summaryreport/en/]). The H1N1 virus was the second virus to originate with the 1918 virus, following the Russian influenza virus in 1977 (4). In the case of the Russian influenza in early 1978, most of the isolates in South America exhibited antigenic drift away from the prototype virus, A/USSR/90/77 (5). However, from 2009 to 2013, no antigenic drift was observed for the pdm09 virus, although isolates with amino acid substitutions in their antigenic sites were detected (6, 7). In 2010, viruses with double mutations in HA (N142D/E391K) were found with increased frequency in the Southern Hemisphere (7), and it was suggested that the double mutations N142D/E391K and N142D/N173K might be associated with a reduction in the ability of vaccine sera to recognize the pdm09 virus (7, 8). Furthermore, the N173K mutation has been shown to emerge under vaccine-induced immune pressure in a ferret model of contact transmission (9). However, such viruses had not been dominant until 2013.

Antigenic mapping of H1 subtype HA was performed on A/PR/8/34 HA (PR8 HA) using variants selected by monoclonal

Received 16 May 2014 Accepted 7 August 2014
Published ahead of print 13 August 2014
Editor: A. García-Sastre
Address correspondence to Eri Nobusawa, nobusawa@nih.go.jp.
* Present address: Yasuko Tsunetsugu-Yokota, Tokyo University of Technology, Tokyo, Japan; Kazuo Kobayashi, Sakai City Institute of Public Health, Osaka, Japan.
Copyright © 2014, American Society for Microbiology. All Rights Reserved.
doi:10.1128/JVI.01381-14

antibodies (MAbs), revealing the existence of four major antigenic sites, Sa, Sb, Ca, and Cb, in HA1 (10, 11). HAs of the pdm09 and A/PR/8/34 viruses originate with the Spanish influenza virus. However, pdm09 HA is directly derived from an American "triple reassortant" possessing the HA of classical swine influenza viruses (12); therefore, the antigenic regions of pdm09 HA and PR8 HA are not necessarily identical. To take precautions against antigenic drift of the pdm09 virus in the near future, it is important to determine the precise antigenic structure of pdm09 HA. In response to the 2009 pandemic, several groups elucidated the antigenic region of pdm09 HA using HA MAbs; however, a systemic analysis of the epitopes has not previously been performed (13–16).

In this study, to precisely identify antigenic regions, we have selected escape mutants of A/Narita/1/2009, the first isolate of the pdm09 virus in Japan, using 16 anti-HA MAbs. For systemic analysis of the epitopes of each MAb, we generated several parent viruses, as we did in our previous study, by considering the mutation rate during the growth of a plaque (17, 18). Thus, by using one MAb, we obtained a maximum of nine escape mutants possessing a single mutation at different positions. Finally, we isolated 599 escape mutants and identified the components of the epitopes of the 16 MAbs at four antigenic sites by cross-reactions of the escape mutants with anti-A/Narita/1/2009 HA MAbs.

TABLE 1 Characterization of MAbs and selection frequencies of escape mutants

MAb[a]	HI titer[b]	NT_{50}[c]	Selection frequency ($-\log_{10}$)[d]			
			P1	P2	P3	P4
n2	1,280	8,000	4.41	4.54	4.29	4.06
n3	25,600	80,000	4.15	4.64	4.57	4.11
n4	25,600	80,000	3.14	4.30	4.30	3.83
n5	12,800	40,000	3.11	4.27	4.23	4.22
n6	3,200	20,000	3.13	4.40	3.99	4.21
n7	640	2,000	3.05	4.40	4.02	3.57
n8	160	400	2.97	4.22	4.09	3.75
n9	12,800	40,000	3.28	4.13	3.79	3.70
n10	6,400	20,000	3.41	3.85	3.89	3.62
n11	1,600	10,000	3.07	3.86	3.76	3.60
n12	25,600	100,000	4.08	3.96	4.32	4.13
n13	640	4,000	3.30	3.77	3.44	3.58
n15	25,600	1,600	4.02	4.40	3.03	3.38
n16	25,600	16,000	4.19	4.69	3.74	3.27
n17	25,600	100,000	4.00	4.84	4.37	4.02
n18	12,800	80,000	4.00	4.31	4.06	4.76

[a] Nomenclatures for each MAbs are described in Text.
[b] An HI test was performed on A/Narita/1/2009 with 0.5% turkey erythrocytes. The HI titer was expressed as the reciprocal of the highest antibody dilution which completely inhibited hemagglutination.
[c] Fifty percent neutralization titers (NT_{50}s) are presented as reciprocals of the highest antibody dilution causing a >50% plaque reduction, as described in the text.
[d] Tenfold serial dilutions of each parent virus (P1 to P4) were mixed with 10-fold dilutions of each MAb. Escape mutants were isolated at the indicated frequency.

MATERIALS AND METHODS

Viruses and cells. A/Narita/1/2009, a pdm09 virus, was isolated from MDCK cells and embryonated chicken eggs, which were infected with a clinical sample. The amino acid sequences of HA genes of the MDCK isolate (accession no. ACR09395) and egg isolate (accession no. ACR09396) viruses are identical. In this study, the MDCK isolate virus was propagated in MDCK cells in Dulbecco's modified Eagle medium supplemented with 0.3% bovine serum albumin and 2 μg/ml acetyl-trypsin (Sigma). Four different clones, P1, P2, P3, and P4, were obtained from well-isolated plaques of MDCK cells infected with A/Narita/1/2009 and used as parent viruses. The amino acid sequence of each parent HA was identical to that in the database (accession number ACR09395). Subsequently, seven pdm09 viruses isolated from MDCK cells from clinical samples were used for antigenic analysis: A/Yamagata/232/2009 (accession no. AB601602), A/Yamagata/752/2009 (AB601604), A/Yamagata/143/2010 (AB601605), A/Yamagata/203/2011 (AB898075), A/Yamagata/206/2011 (AB898076), A/Yamagata/264/2012 (AB898077), and A/Yamagata/87/2013 (AB898078). To examine the cross-reactivity of MAbs with seasonal H1N1 virus HA, purified HA proteins of A/Solomon Islands/3/2006 and A/Brisbane/59/2007 (Denka Seiken Co., Ltd., Tokyo, Japan) were used.

Antibodies. BALB/c mice were subcutaneously primed with 20 μg of inactivated A/Narita/1/2009 virus twice within a 3-week interval, and splenocytes were fused with Sp2/O myeloma cells at day 3 after the boosting. After limiting serial dilutions, hybridoma cells binding to A/Narita/1/2009 HA but not to A/Brisbane/59/2007 HA (H1N1) were selected by enzyme-linked immunosorbent assay (ELISA). This study was approved by the Institutional Animal Care and Use Committee of the National Institute of Infectious Diseases, Japan, and all mice were used in accordance with their guidelines.

In this study, we characterized the epitopes of the following 16 monoclonal antibodies (MAbs): NSP18 (n2), NSP30 (n3), NSP21 (n4), NSP2 (n5), NSP19 (n6), NSP22 (n7), NSP24 (n8), NSP20 (n9), NSP6 (n10), NSP26 (n11), NSP11 (n12), NSP8 (n13), NSP29 (n15), NSP27 (n16), NSP17 (n17), and NSP10 (n18). Postinfection ferret antiserum against A/California/7/2009 was used for serological assays.

Neutralization test. The virus neutralization test was performed using 6-well microplates. Mixtures of 2-fold serial dilutions of each MAb and 100 PFU of A/Narita/1/2009 were incubated for 30 min at 37°C and used to inoculate MDCK cells. After 1 h, an agar overlay medium was added, and the cells were incubated at 37°C for 3 days. Neutralization titers are presented as reciprocals of the highest antibody dilution causing a >50% reduction of plaque number in 100 PFU of A/Narita/1/2009 virus.

Selection of escape mutants. The escape mutants were selected by incubating each parent virus with MAbs against A/Narita/1/2009 HA, essentially following the procedure of a previous study (17, 19). Briefly, a 10-fold serial dilution of each parental virus (P1, P2, P3, and P4) was mixed with an equal volume of a 1:10 dilution of ascites fluid containing MAbs. After incubation for 30 min at room temperature, the virus-antibody mixture was inoculated onto the MDCK cells and an agar overlay medium was added. Ten nonneutralized plaque viruses per experiment were isolated and amplified in MDCK cells. The nucleotide sequence of each mutant HA gene was determined, and the deduced amino acid sequence was compared with that of A/Narita/1/2009 HA. The antigenic character of each isolate was examined using a hemagglutination inhibition (HI) test.

Nucleotide sequencing. The nucleotide sequences of the HA genes were directly determined from RT-PCR products using the ABI Prism 3130 sequencer (Applied Biosystems). The sequences of HA primers will be provided upon request.

Radioisotope labeling and immunoprecipitation. Monolayers of MDCK cells infected with stock virus were incubated with (+TM) or without (−TM) tunicamycin (2 μg/ml) at 37°C. At 7 h postinfection, the cells were pulsed for 30 min (−TM) or 60 min (+TM) with 4 MBq/ml [^{35}S]methionine (ARC) and then disrupted as described previously (19). Immunoprecipitates of MAb n17 were analyzed by SDS-PAGE on 15% gels containing 4 M urea and processed for analysis by fluorography.

RESULTS

Selection of escape mutants of A/Narita/1/2009. We have generated 16 MAbs with neutralizing activity against A/Narita/1/2009 HA. The HI titers and neutralization titers of the MAbs are shown in Table 1. To localize the antigenic sites on pdm09 HA, we se-

lected escape mutants of the A/Narita/1/2009 strain using these MAbs. Four parent viruses (P1, P2, P3, and P4) were neutralized with each of the 16 MAbs, and nonneutralized plaque viruses were then analyzed as described in Materials and Methods. Escape mutants resistant to each MAb were isolated with a frequency ranging from $10^{-2.97}$ to $10^{-4.84}$ (Table 1). Consequently, we isolated 599 escape mutants with a single amino acid substitution in the HA1 domain; 157, 147, 148, and 147 mutants were derived from P1, P2, P3, and P4, respectively. These mutants were classified into 43 groups, which had different amino acid substitutions at 24 positions. By neutralizing the parent viruses derived from more than one plaque, we were able to obtain various mutants carrying different mutations (Table 2).

Antigenic sites revealed by reactivities of MAbs with escape mutants in HI tests. In Fig. 1, the 24 positions are shown on the primary sequence of A/Narita/1/2009 HA1 and compared with the corresponding positions within 1918 Spanish influenza virus HA, seasonal H1N1 virus HA, and A/PR/8/34-Mt. Sinai strain HA (PR8-Mt.Sinai HA) (10).

The reactivity of each MAb with the panel of escape mutants was examined using an HI test (Table 2). Based on their reactivities, the MAbs were assembled into four complementary groups: Sa (n3 to n13), Sb (n15 and n16), Ca2 (n17 and n18), and n2.

(i) Site Sa. Single amino acid changes at positions 141, 142, 171, 172, and 180 in the Sa site affected the reactions of the mutants with MAbs n3 to n8, whereas the reactivities of MAbs n9 to n13 with the mutants was affected by amino acid substitutions at positions 141, 142, 171, 172, and 177 (except for n13) at site Sa. Further mutations at positions 143 and 174 in the Sa site and position 173 in the Sb site affected the reactivity with n4 to n6, n4 to n10, and n9 to n13, respectively. MAbs n9 and n10 lost reactivity when mutations were present at position 173, whereas n11 to n13 reacted with N173I but not with N173D. These results indicate that (i) the Sa site of Narita HA is composed of the residues at positions 141, 142, 143, 171, 172, 173, 174, 177, and 180, and (ii) there are two distinct regions in the Sa site that are recognized differently by MAbs n3 to n8 and MAbs n9 to n13 (Tables 2 and 3).

(ii) Site Sb. Mutations at positions 170, 173, 202, 206, 210, 211, and 212 in site Sb affected reactivity with n15 and n16. Interestingly, n15 showed decreased reactivity with G172V (Sa site) but reacted with G172E. Similar to residue 173, residue 172 also belonged to epitopes in sites Sa and Sb, depending on the amino acid residue (Tables 2 and 3).

In this study, single-mutation mutants containing H143Y (Sa site) or Q210E or N211D (Sb site) did not react with MAbs n4 to n6, n15, or n15/n16, respectively, as shown in the HI test. However, they reacted well with MAbs n7, n11, and n10/n11, respectively, even these MAbs were used for the selection of those mutants (Table 2).

(iii) Site Ca2. In this study, two epitopes of n17 and n18 were identified in the Ca2 site. The HI reactivity of n17 and n18 with each escape mutant indicated that their epitopes are composed of residues at positions 151, 154, 156, 157, 158, 159, 200, and 238; however, the reactivity of each MAb differed based on the substituted amino acid residue, which implies that the amino acid sequences are different for the paratope of each MAb (Tables 2 and 3).

(iv) Site Pa. Three escape mutants, each possessing a single mutation at position 147, 170, or 172, were selected by MAb n2. Moreover, n2 showed decreased reactivity with the other mutant, carrying a K159N change, which was selected by n17 (Table 2). The n2 epitope presumably consisted of the residues at positions 147, 159, 170, and 172, and the last three residues were located in the Ca2, Sb, and Sa sites, respectively (Table 3). A similar epitope consisting of residues K136, D144, K147, G148, K171, and G172 has been identified for the human monoclonal antibody EM4C04, which was derived from a patient infected with the pdm09 virus (13, 15). We designated this novel antigenic site Pa.

The reactivity of ferret antiserum against A/California/7/2009 with the representative escape mutants related to each antigenic site was also examined by the HI test. No mutants showed reduced reactivity with the polyclonal ferret antiserum compared to that of the parent virus (Table 2).

Characteristics of the antigenic structure of pdm09 HA. Figure 2 shows the antigenic sites of A/Narita/1/2009 HA (Fig. 2). The epitopes for the investigated MAbs, except for epitope n2, were localized within the Sa, Sb, and Ca2 antigenic sites. In this study, no MAbs against Ca1 or Cb were identified. The unique positions of the amino acid substitutions in the escape mutants of A/Narita/1/2009 were 147 and 200. In the three-dimensional (3-D) structure, residue 200 of site Ca2 was located next to the residues of site Sb but was far from the other components of site Ca2 in the 3-D structure (Fig. 2). Although the S200P mutation affected the reactivity with n17 and n18, this influence may be attributed to a conformational change at topologically distant sites rather than to a direct interaction between the epitope and the paratope.

Residue 147 is located near the right edge of the receptor-binding site and is near the other members of epitope n2, including residues 159, 170, and 172, in the 3-D structure. This epitope was not detected in the antigenic site of PR8-Mt. Sinai HA or several seasonal influenza viruses (H1N1) that circulated during and after 1994/1995 because of the lack of residue 147. However, because of the presence of residue 147, the Pa site may exist in the Spanish influenza virus, PR8-Cambridge strain, and seasonal H1N1 viruses that were isolated before 1994.

Acquisition of a glycosylation site is known to shield epitopes from antibody recognition. In the seasonal influenza H1N1 virus, two highly conserved glycosylation sites, at positions 142 and 177, were identified in the Sa site, but both sites were absent in pdm09 HA. In this study, a new oligosaccharide attachment site, K177N, was generated in an escape mutant that was selected by MAbs n10 and n11. However, this mutant and others with K177T or K177E all reacted with the MAbs targeting site Sa. Thus, to determine whether the HA mutant with K177N was modified with N-linked glycans, we compared the electrophoretic mobilities of the mutant HAs, i.e., those with K177N and K177T, in SDS-polyacrylamide gels. As shown in Fig. 3, in the absence of TM, the parental virus and both mutant HAs showed slower electrophoretic mobility than in the presence of TM, but the mobility of these HAs was similar, suggesting that an additional glycosylation did not occur at position 177 in the mutant carrying N177.

Antigenic characterization of pdm09 HA viruses from 2009 to 2013. To detect signs of antigenic drift, genetic and antigenic analyses have been extensively performed for pdm09 isolates obtained from 2009 to 2013 (6–8). Compared with the pdm09 virus,

TABLE 2 Amino acid mutations in HAs of escape mutants with their isolation efficiencies and their effects on reactivity with each MAb

Amino acid change of escape mutants	No. of escape mutants derived from parent virus					MAb(s) used for selection of escape mutants	Hemagglutination inhibition titer of MAb[a] or of ferret antiserum against pdm09 virus																	
							MAb at site:																	
							Sa											Sb		Ca2		Pa;	Ferret antiserum against A/ California/7/2009
	P1	P2	P3	P4	Total		n3	n4	n5	n6	n7	n8	n9	n10	n11	n12	n13	n15	n16	n17	n18	n2	
None (parent virus [P3])							12,800	12,800	12,800	3,200	640	160	12,800	6,400	2,560	25,600	640	25,600	25,600	25,600	25,600	640	1,280
P141T		3		2	5	n9, n10, n11, n13	—	—/0	—	—	—	—	0	0	0	0	0	—	—	—	—	—	NT[b]
P141L		3		3	6	n3, n8, n12	0	0	0	0	0	0	0	0	0	0	0	—	—	—	—	—	NT
N142D	10	3	10	2	25	n3, n4, n6, n7, n9, n11, n12	0	0	0	0	0	0	0	0	0	0	0	—	—	—	—	—	1,280
H143Y			2		2	n7	—	0	0	0	—	—	—	—	—	—	—	—	—	—	—	—	NT
K171E	1	3	11		15	n4–n9, n11, n12	—/0	0	0	0	0	0	0	0	0	0	0	—	—	—	—	—	NT
K171N		8	8	25	41	n3–n13	—/0	0	0	0	0	0	0	0	0	0	0	—	—	—	—	—	1,280
K171T		2	1	6	9	n3, n4, n9, n10, n12, n13	—/0	0	0	0	0	0	0	0	0	0	0	—	—	—	—	—	NT
K171Q		5			5	n12, n13	—	0	0	0	0	0	0	0	0	0	0	—	—	—	—	—	NT
G172E	40	71	45	52	208	n2, n3–n13	0	0	0	0	0	0	0	0	0	0	0	—	—	—	—	—/0	1,280
G172V	3	4			7	n12	0	0	0	0	0	0	0	0	0	0	0	0	—	—	—	—	NT
S174L	51		1	1	53	n4–n11	—	0	0	0	0	0	0	0	—	—	—	—	—	—	—	—	NT
K177N		2	1	1	4	n10, n11	—	—	—	—	—	—	—/0	0	—	0	—	—	—	—	—	—	NT
K177T	1	2			3	n11–n13	—	—	—	—	—	—	0	0	—/0	0	—	—	—	—	—	—	2,560
K177E		1		2	3	n10	—	—	—	—	—	—	0	0	—/0	0	—	—	—	—	—	—	NT
K180E		1		1	2	n3, n7	0	0	0	0	0	0	—	—	—	—	—	—	—	—	—	—	1,280
K180N				1	1	n7	0	0	0	0	0	0	—	—	—	—	—	—	—	—	—	—	NT
K170E	2	3	10	3	18	n2, n6, n8, n15, n16	—	—	—	—	—	—	—	—	—	—	—	0	0	—	—	—/0	NT
K170Q		1			1	n16	—	—	—	—	—	—	—	—	—	—	—	0	0	—	—	—	NT
K170T		1			1	n15	—	—	—	—	—	—	—	—	—	—	—	0	0	—	—	—	NT
N173I	2	1			3	n9, n15	—	—	—	—	—	—	0	0	0	0	0	0	0	—	—	—	640
N173D	1	6	29	5	41	n9–n11, n13, n15, n16	—	—	—	—	—	—	0	0	—/0	—	—	0	0	—	—	—	NT
S202N		2			2	n16	—	—	—	—	—	—	—	—	—	—	—	0	0	—	—	—	1,280
Q206E			11	1	12	n15, n16	—	—	—	—	—	—	—	—	—	—	—	0	0	—	—	—	NT
Q210L		1			1	n15	—	—	—	—	—	—	—	—	—	—	—	0	0	—	—	—	NT
Q210E				1	1	n11	—	—	—	—	—	—	—	—	—	—	—	0	—	—	—	—	NT
N211D	9				9	n10, n11	—	—	—	—	—	—	—	—	—	—	—	0	0	—	—	—	NT
A212E	17	5	3	18	43	n15, n16	—	—	—	—	—	—	—	—	—	—	—	0	0	—	—	—	2,560
A151V			1		1	n17	—	—	—	—	—	—	—	—	—	—	—	—	—	0	—	—	NT
A151G	2			3	5	n17, n18	—	—	—	—	—	—	—	—	—	—	—	—	—	0	0	—	640
P154S		1	2	1	4	n18	—	—	—	—	—	—	—	—	—	—	—	—	—	—/0	0	—	NT
P154T			2		2	n18	—	—	—	—	—	—	—	—	—	—	—	—	—	—	0	—	NT
A156V		1			1	n17	—	—	—	—	—	—	—	—	—	—	—	—	—	0	—	—	NT
A156T			1	4	5	n17	—	—	—	—	—	—	—	—	—	—	—	—	—	0	—	—	NT
A156D		5	4	4	13	n17, n18	—	—	—	—	—	—	—	—	—	—	—	—	—	0	0	—	NT
G157E	15	8	4	3	30	n17, n18	—	—	—	—	—	—	—	—	—	—	—	—	—	0	0	—	NT
G157R	1				1	n18	—	—	—	—	—	—	—	—	—	—	—	—	—	—	0	—	NT
A158E		2			2	n17, n18	—	—	—	—	—	—	—	—	—	—	—	—	—	0	0	—	1,280
A158V				1	1	n18	—	—	—	—	—	—	—	—	—	—	—	—	—	—	0	—	NT
K159N	2				2	n17	—	—	—	—	—	—	—	—	—	—	—	—	—	0	0	0	1,280
S200P			1	1	2	n17, n18	—	—	—	—	—	—	—	—	—	—	—	—	—	0	—/0	—	1,280
R238K				2	2	n18	—	—	—	—	—	—	—	—	—	—	—	—	—	—	—/0	—	NT
K147N		2	1		3	n2	—	—	—	—	—	—	—	—	—	—	—	—	—	—	—/0	0	NT
K147Q				4	4	n2	—	—	—	—	—	—	—	—	—	—	—	—	—	—	—/0	0	2,560
Total no. of mutants	157	147	148	147	599																		

[a] An HI test was performed with 0.5% turkey erythrocytes. The HI titer was expressed as the reciprocal of the highest antibody dilution which completely inhibited hemagglutination. —, 2- to 4-fold-lower or -higher HI titer than that with the parent virus. —/0, 8-fold lower HI titer than that with the parent virus. 0, at least 16-fold lower HI titer than that with the parent virus.

[b] NT, not tested.

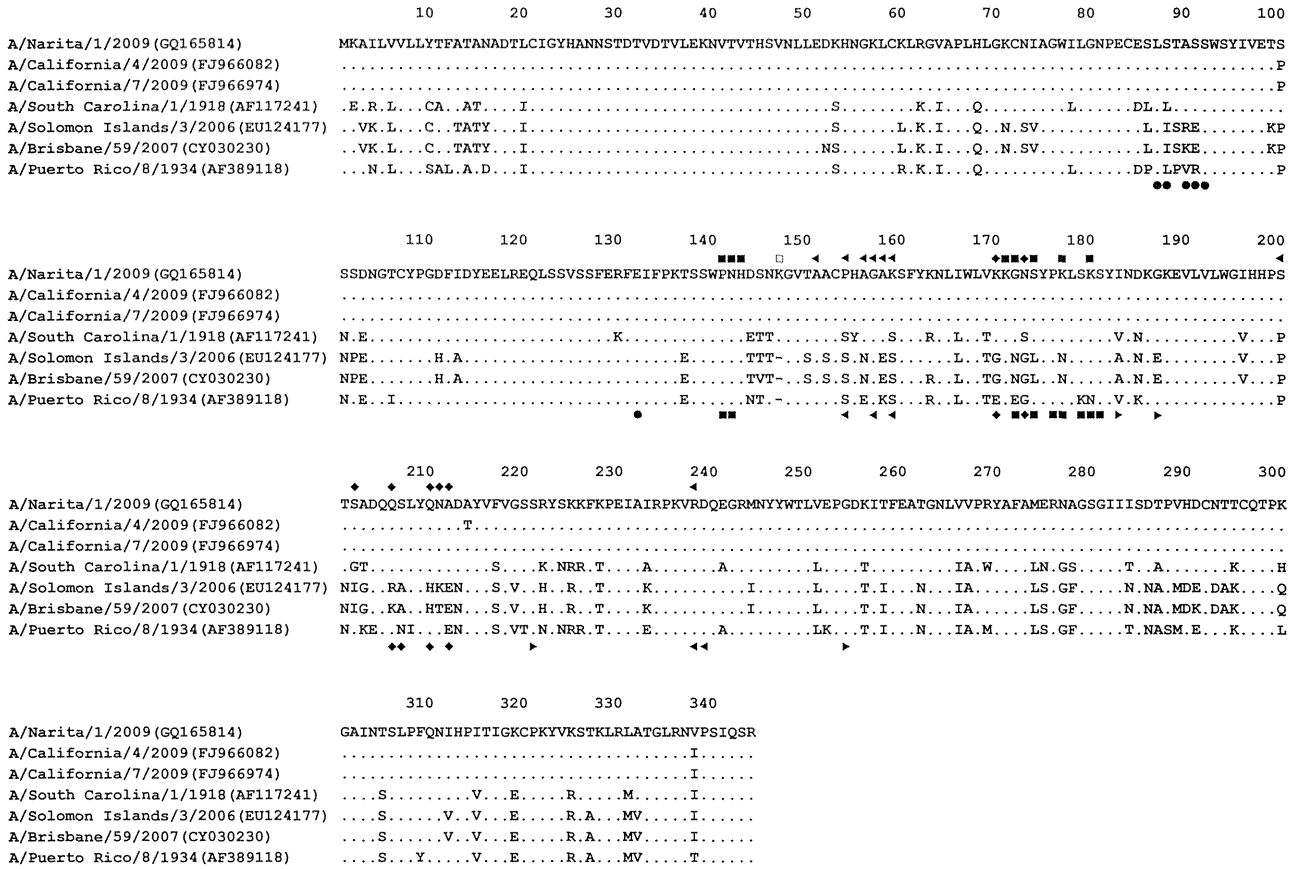

FIG 1 Comparison of the antigenic sites of HA1 among H1N1 viruses. Alignments of the amino acid sequences of the HA1 region of A/Narita/1/2009 (GenBank accession no. ACR09395), A/California/4/2009 (FJ966082), A/California/7/2009 (FJ966974), A/South Carolina/1/1918 (AF117241), A/Solomon Islands/3/2006 (EU124177), A/Brisbane/59/2007 (CY030230), and A/Puerto Rico/8/1934 (Mt. Sinai) (AF389118) are shown using H1 numbering from the first methionine in the signal peptide. Each antigenic site is shown with the corresponding symbol: ■, Sa; ◆, Sb; ▶, Ca1; ◀, Ca2; ●, Cb; □, Pa. Symbols for A/Narita/1/2009 and A/Puerto Rico/8/1934 are shown above and below the sequence, respectively.

various mutations were found at the antigenic sites of these natural isolates; however, significant antigenic differences from the A/California/7/2009 vaccine strain were not found when using ferret antiserum against A/California/7/2009 (6, 7).

To confirm that the mutations in the antigenic sites of the natural isolates affected the reactivities of the corresponding MAbs, cross-reactions of the MAbs were investigated using natural isolates obtained in Yamagata Prefecture, Japan, from 2009 to 2013. Table 4 shows the reactivities of the representative MAbs with seven representative pdm09 isolates. Among the isolates from 2009/2010, A/Yamagata/232/2009 and A/Yamagata/143/2010 reacted well with all of the investigated MAbs, whereas A/Yamagata/752/2009 failed to react with MAbs to site Sa and showed an 8-fold-lower reactivity with n2 than did A/Narita/1/2009, possibly because of the G172E mutation (sites Sa and Pa). Two other isolates from 2010-2011, A/Yamagata/203/2011 and A/Yamagata/206/2011, exhibited no or decreased reactivity with n17/n18 and n16, respectively, possibly because of the A151T/A158S/S200P (site Ca2) and S202T (site Sb) mutations. Two isolates obtained in 2012-2013, A/Yamagata/264/2012 and A/Yamagata/87/2013, showed low reactivity with n16 and n3/n7/n16, presumably because of S202T (site Sb) and K180I/S202T (site Sa/Sb), respectively.

To determine whether any MAbs exhibit cross-reactivity with seasonal H1N1 viruses, we also examined the reactivities of 16 MAbs with A/Solomon Island/3/2006 and A/Brisbane/59/2007 HAs. No MAbs reacted well with these seasonal H1N1 virus HAs (Table 4).

During 2009 to 2013, amino acid changes at positions 202 and 220 were found in the main stream of the evolutionary pathway of these natural isolates of HA1 in Yamagata Prefecture (Fig. 4). According to the antigenic analysis of the viruses shown in Table 4, n16 lost reactivity with a S202T mutant, whereas the other mutation, S220T, which is located in the Ca1 site of PR8 HA, did not affect the reactivities of the viruses with the MAbs that were used in this study. These results show that the mutations in the antigenic site of the natural variants predictably affected reactivity with their corresponding MAbs. However, no variant lost reactivity with the ferret postinfection antiserum against A/California/7/2009, as observed for the several escape mutants in this study (Table 2). The antibodies produced in the naive ferret infected with A/California/7/2009 therefore presumably recognize more than one antigenic site of HA.

TABLE 3 Amino acid substitutions of escape mutants HAs which affect reactivity with each MAb

MAb	Amino acid substitution(s)[a] in each antigenic site			
	Sa site	Sb site	Ca2 site	Pa site
n3	P141L; N142D; K171E; K171N; K171T; G172E; G172V; K180E; K180N			
n4	P141T; P141L; N142D; H143Y; K171E; K171N; K171T; K171Q; G172E; G172V; S174L; K180E; K180N			
n5	P141L; N142D; H143Y; K171E; K171N; K171T; K171Q; G172E; G172V; S174L; K180E; K180N			
n6	P141L; N142D; H143Y; K171E; K171N; K171T; K171Q; G172E; G172V; S174L; K180E; K180N			
n7	P141L; N142D; K171E; K171N; K171T; K171Q; G172E; G172V; S174L; K180E; K180N			
n8	P141L; N142D; K171E; K171N; K171T; K171Q; G172E; G172V; S174L; K180E; K180N			
n9	P141T; P141L; N142D; K171E; K171N; K171T; K171Q; G172E; G172V; S174L; K177N; K177T	N173I; N173D		
n10	P141T; P141L; N142D; K171E; K171N; K171T; K171Q; G172E; G172V; S174L; K177N; K177T	N173I; N173D		
n11	P141T; P141L; N142D; K171E; K171N; K171T; K171Q; G172E; G172V; K177T; K177E	N173I; N173D		
n12	P141T; P141L; N142D; K171E; K171N; K171T; K171Q; G172E; G172V; K177N; K177T; K177E	N173I		
n13	P141T; P141L; N142D; K171E; K171N; K171T; K171Q; G172E; G172V	N173I		
n15	G172V	K170E; K170Q; K170T; N173I; N173D; S202N; Q206E; Q210L; Q210E; N211D; A212E		
n16		K170E; K170Q; K170T; N173I; N173D; S202N; Q206E; Q210L; N211D; A212E		
n17			A151V; A151G; P154S; A156V; A156T; A156D; G157E; A158E; K159N; S200P	
n18			A151G; P154S; P154T; A156D; G157E; G157R; A158E; A158V; K159N; S200P; R238K	K147N; K147Q
n2	G172E	K170E	K159N	K147N; K147Q

[a] All mutations that decreased the HI titer of each MAb at least 8-fold compared to the titer with the parent virus.

DISCUSSION

The prototypes of the pdm09 virus are A/California/4/2009 (MDCK isolate) and A/California/7/2009 (egg isolate). The primary sequence of A/Narita/1/2009 HA1 is similar to that of the prototype viruses (Fig. 1). HA1 from A/Narita/1/2009 differs from A/California/4/2009 and A/California/7/2009 by two amino acids and one amino acid, respectively. These differences were not observed in the antigenic region, and the reactivity of the ferret antiserum against A/California/7/2009 is similar among those viruses (data not shown). Therefore, we have analyzed the antigenic structure of HA of A/Narita/1/2009, as a representative pdm09 virus, using 16 anti-HA MAbs and their escape mutants. Most epitopes of the MAbs were located in the antigenic sites Sa, Sb, and Ca2. In addition, epitope n2 was defined in a novel antigenic site (Pa) and was proximal to the receptor-binding site (Fig. 2).

Based on the antigenic analysis of PR8-Mt. Sinai HA, sites Sa and Sb are defined as operationally distinct areas that are separated by residues 170/173 of the Sb site and 172/174 of the Sa site, which lie in the same region of the polypeptide chain (10). Although sites Sa and Sb are contiguous and have been suggested to share a close linkage, simultaneous binding of antibodies to each site has not been identified (10, 11, 20). However, a study of the crystal structure of human MAb 2DI in complex with the 1918 pandemic HA demonstrated that the epitope of MAb 2DI, which is derived from survivors of the 1918 pandemic, contained the residues at positions 142 (in the Sa site) and 171 to 183 (in the Sa

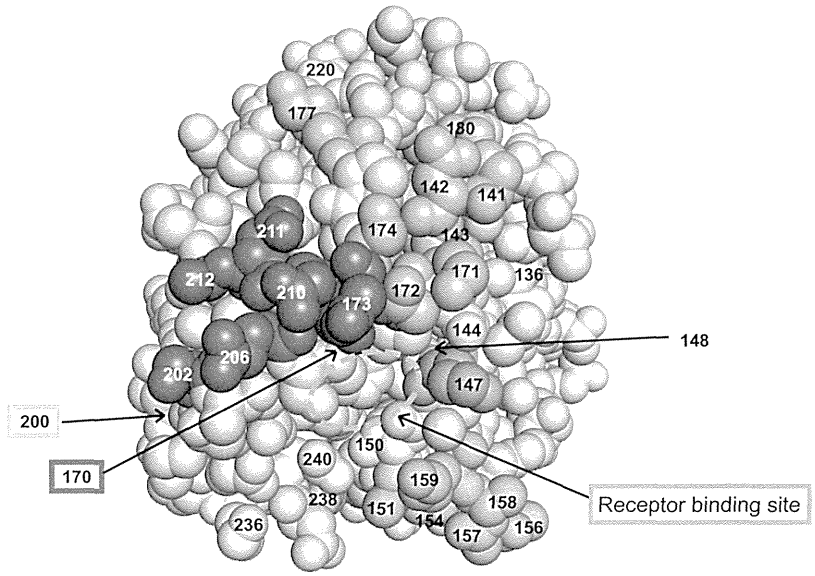

FIG 2 Antigenic structure of HA of A/Narita/1/2009. Positions of amino acid changes in the escape mutants are located on the globular head of HA of A/Narita/1/2009, shown with numbering. The three-dimensional structure of A/Narita/1/2009 HA was generated by the protein structure homology-modeling server "SWISS MODEL" using the coordinates of A/California/4/2009 (PDB ID 3al4A). The image was created using the software program PyMOL. The residues at each antigenic site are colored as pink for the Sa site, sky blue for the Sb site, green for the Ca2 site, and orange for residue 147. The residues discussed in the text are colored yellow.

and Sb sites). Similarly, in this study, epitopes of mouse MAbs n9 to n13 and n15 were composed of residues in the Sa and Sb sites (16).

Based on the residues of epitopes n2 and EM4C04 (13), we have determined that the novel antigenic site (Pa) of pdm09 HA is between sites Sa, Sb, and Ca2 and residue 147. In a previous study using mouse MAbs, this epitope in the Pa site was not identified in PR8-Mt. Sinai HA (20). We therefore considered that the Pa antigenic site may be specific to pdm09 HA. Recently, epitopes of broadly neutralizing human MAbs, i.e., 5J8 and CH65, were found around the receptor-binding site (15, 16). MAb 5J8 was derived from a healthy, middle-aged woman and had HI activity against A/South Carolina/1/1918 and A/California/4/2009. Epitope 5J8 is composed of residues 147, 151, and 236, which are near epitope n2. Because residue 151 is near residue 159, epitope 5J8 may partially overlap epitope n2 and comprise the Pa site. In contrast, MAb CH65 was obtained by rearranging the heavy- and light-chain genes derived from a subject immunized with the 2007 trivalent vaccine, including the seasonal H1N1 virus lacking residue 147 of HA. The crystal structure of the complex between CH65 and A/Solomon Islands/3/2006 HA, which had a deletion of residue 147, suggested that residues 150, 151, and 240, which were located on the right edge of the receptor-binding site, were involved in the interaction. A neutralization assay showed that among the historical H1N1 viruses, the viruses with an insertion at position 147 were resistant to CH65. Taking these results into consideration, the region around position 147 is presumably a component of epitopes for human antibodies against H1HA. Considering the location of residue 147, a mutation at this position may significantly affect the receptor-binding ability. However, in this study, two escape mutants of Narita/1/2009, carrying the mutations K147N and K147Q, were isolated using MAb n2. In another study, a similar escape mutant of A/California/4/2009, with K147Q, was selected by human MAb 5J8 (15). During the circulation of the H1N1 seasonal influenza viruses in 1947 to 1957 and 1977 to 1995, only mutations K to R and R to K were recognized, and residue 147 was deleted after 1995. Similarly, residue 144, which is located near position 147 of older H1N1 viruses, was also deleted immediately before the disappearance of these viruses in 1957 (21). Deletions of residues in close proximity to the receptor-binding site of HA seem preferable for the escape of H1N1 viruses from immune selection in the human population. It is well known that the glycosylation of HA prevents its neutralization by antibodies. A previous study implied that pdm09 HA modified with additional glycosylation sites at positions 142 and 177 was resistant to neutralization by antibodies to wild-type HA (22). Therefore, glycosylation at these positions has implications for the antigenic drift of pdm09 viruses. However, as indicated in this study, the asparagine at position 177 was not glycosylated, even though the mutation affected reactivity with the MAb.

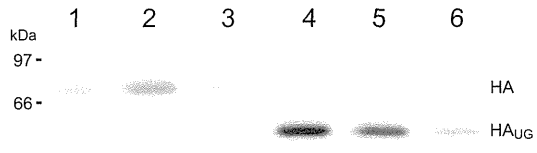

FIG 3 Immunoprecipitation analysis of the HA molecules of escape mutants carrying amino acid substitutions at position 177. MDCK cells infected with parental virus (lanes 1 and 4) and mutants with the K177T (lanes 2 and 5) and K177N (lanes 3 and 6) substitutions were labeled with [^{35}S]methionine for 30 min in the absence of tunicamycin (lanes 1 to 3) or for 60 min in the presence of tunicamycin (lanes 4 to 6) at 7 h postinfection. Cells were immunoprecipitated with MAb n17 to site Ca2, and the resulting precipitates were analyzed by SDS-PAGE.

TABLE 4 Antigenic analysis of pdm09 natural isolates in Yamagata Prefecture and seasonal H1N1 viruses using representative MAbs

Virus strain	Amino acid change(s)[a]	HI titer[b]							
		MAbs of respective antigenic site							
		Sa			Sb	Ca2		Pa	Postinfection ferret antiserum against A/California/7/2009
		n3	n7	n10	n16	n17	n18	n2	
pdm09 natural isolates									
A/Narita/1/2009		12,800	640	6,400	25,600	25,600	25,600	640	1,280
2009-2010 season									
A/Yamagata/232/2009	S220T	6,400	320	3,200	25,600	12,800	12,800	640	1,280
A/Yamagata/752/2009	G172E, K188R, S220T, A214T	<[c]	<	<	6,400	6,400	3,200	80	640
A/Yamagata/143/2010	V36I, D52G, A203T, S220T	12,800	320	3,200	12,800	12,800	25,600	320	640
2010-2011 season									
A/Yamagata/203/2011	V64I, A151T, A158S, S200P, S220T, I312V	6,400	640	6,400	12,800	<	160	640	1,280
A/Yamagata/206/2011	K136N, S160G, S202T, S220T, A214T	6,400	640	6,400	1,600	2,560	2,560	640	1,280
2012-2013 season									
A/Yamagata/264/2012	D114N, S202T, S220T, F227S, V251I, K300E	6,400	320	1,600	320	12,800	12,800	320	640
A/Yamagata/87/2013	S101G, S160G, K180I, S202T, A214T, S220T	20	80	1,600	320	12,800	12,800	320	640
Seasonal H1N1 viruses[d]									
A/Solomon Islands/3/2006		<	<	<	<	40	20	<	NT[e]
A/Brisbane/59/2007		<	<	<	<	<	<	<	NT

[a] Amino acid differences in HA1 between pdm09 natural isolates and A/Narita/1/2009 are shown.
[b] The HI test was performed with 0.5% turkey erythrocytes. The HI titer is expressed as the reciprocal of the highest antibody dilution which completely inhibited hemagglutination.
[c] <, less than 20.
[d] Amino acid sequences of seasonal H1N1 viruses are shown in Fig. 1.
[e] NT, not tested.

Amino acid changes at positions 170 to 174 have been identified after the cell culture adaptation of pdm09 viruses (9, 23, 24). In this study, the variants with G172E comprised one-third of all of the mutants. However, each variant lost reactivity with the MAbs that were used for the selection of the variant, suggesting that variants with G172E were not selected during adaptation to MDCK cells.

Since the emergence of the pdm09 virus as a pandemic virus in 2009, stringent surveillance of pdm09 viruses has been applied to detect antigenic variants. From 2009 to 2013, amino acid changes at positions 220 (Ca1 site) and 202 (Sb site) were found in the mainstream of the evolutionary pathway of pdm09 HA (Fig. 4). However, as shown in Table 4, hemagglutination abilities of natural isolates with the mutations S202T and S220T were efficiently inhibited by postinfection ferret sera against the A(H1N1)pdm09 virus. No antigenic differences from the vaccine strain, A/California/7/2009, were reported for the natural isolates in the various region of the world in 2013 (25, 26). In the case of the reappearance of H1N1 viruses in 1977, several antigenic variants, A/Lackland/3/78 and A/Brazil/11/78, showed 4- to 8-fold decreases in reactivity with the postinfection ferret sera against A/USSR/90/77. These variants also failed to react with MAb 264 against A/USSR/90/77 HA (27, 28). Using binding assays of MAb 264 with mutant HA, we have identified E233K as a mutation responsible for the

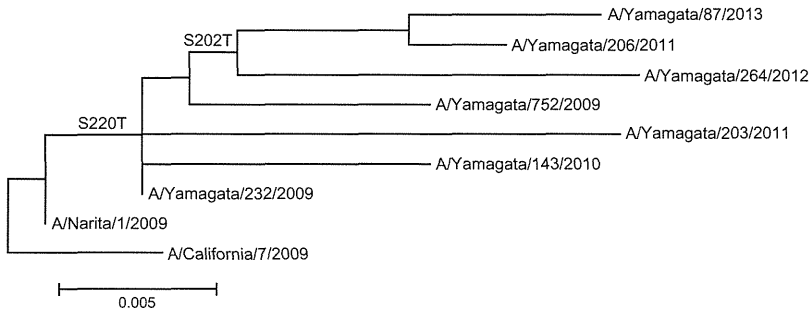

FIG 4 Phylogenetic tree of the HA1 polypeptide of the natural isolates from 2009 to 2013 that were used in this study. A phylogenetic tree was constructed using the neighbor-joining method in the CLUSTAL W software program, version 2.1. Numbers refer to the mainstream amino acid changes that were fixed in most of the subsequent strains.

antigenic drift of A/USSR/90/77 (29). In fact, this mutation was found in the mainstream of the evolutionary pathway (30). It is difficult to identify such a crucial mutation in antigenic variants, which usually possess extra mutations unrelated to antigenicity. In the present study, we identified the residues that composed the epitopes of 16 MAbs against A/Narita/1/2009 HA. The use of such MAbs should be helpful in determining critical amino acid substitutions for the antigenic drift of A(H1N1)pdm09 viruses, once such drift occurs. Consequently, these findings may help the WHO to make recommendations for the next vaccine virus among pdm09 H1N1 viruses.

ACKNOWLEDGMENTS

This study was supported in part by a Health Labor Sciences Research Grant, Research on Emerging and Re-emerging Infectious Diseases (to E.N.; no. H22-//Shinko-Ippan-001//) from the Ministry of Health, Labor and Welfare of Japan.

We are greatly indebted to Katsuhisa Nakajima for helpful suggestions and valuable discussions. We thank Yasushi Suzuki for preparing the image of 3-D structure and Yoko Kadowaki for her assistance with sequence analysis.

We declare that we have no potential conflicts of interests related to this article.

REFERENCES

1. Smith GJ, Vijaykrishna D, Bahl J, Lycett SJ, Worobey M, Pybus OG, Ma SK, Cheung CL, Raghwani J, Bhatt S, Peiris JS, Guan Y, Rambaut A. 2009. Origins and evolutionary genomics of the 2009 swine-origin H1N1 influenza A epidemic. Nature 459:1122–1125. http://dx.doi.org/10.1038/nature08182.
2. World Health Organization. 2010. Recommended viruses for influenza vaccines for use in the 2010-2011 northern hemisphere influenza season. Wkly. Epidemiol. Rec. 85:81–92.
3. World Health Organization. 2011. Influenza A(H1N1) 2009 virus: current situation and post-pandemic recommendations. Wkly. Epidemiol. Rec. 86:61–72.
4. Nakajima K, Desselberger U, Palese P. 1978. Recent human influenza A (H1N1) viruses are closely related genetically to strains isolated in 1950. Nature 274:334–339. http://dx.doi.org/10.1038/274334a0.
5. Kendal AP, Joseph JM, Kobayashi G, Nelson D, Reyes CR, Ross MR, Sarandria JL, White R, Woodall DF, Noble GR, Dowdle WR. 1979. Laboratory-based surveillance of influenza virus in the United States during the winter of 1977-1978. I. Periods of prevalence of H1N1 and H3N2 influenza A strains, their relative rates of isolation in different age groups, and detection of antigenic variants. Am. J. Epidemiol. 110:449–461.
6. Dapat IC, Dapat C, Baranovich T, Suzuki Y, Kondo H, Shobugawa Y, Saito R, Suzuki H. 2012. Genetic characterization of human influenza viruses in the pandemic (2009-2010) and post-pandemic (2010-2011) periods in Japan. PLoS One 7:e36455. http://dx.doi.org/10.1371/journal.pone.0036455.
7. Barr IG, Cui L, Komadina N, Lee RT, Lin RT, Deng Y, Caldwell N, Shaw R, Maurer-Stroh S. 2010. A new pandemic influenza A(H1N1) genetic variant predominated in the winter 2010 influenza season in Australia, New Zealand and Singapore. Euro Surveill. 15:19692.
8. Strengell M, Ikonen N, Ziegler T, Julkunen I. 2011. Minor changes in the hemagglutinin of influenza A(H1N1)2009 virus alter its antigenic properties. PLoS One 6:e25848. http://dx.doi.org/10.1371/journal.pone.0025848.
9. Guarnaccia T, Carolan LA, Maurer-Stroh S, Lee RT, Job E, Reading PC, Petrie S, McCaw JM, McVernon J, Hurt AC, Kelso A, Mosse J, Barr IG, Laurie KL. 2013. Antigenic drift of the pandemic 2009 A(H1N1) influenza virus in A ferret model. PLoS Pathog. 9:e1003354. http://dx.doi.org/10.1371/journal.ppat.1003354.
10. Caton AJ, Brownlee GG, Yewdell JW, Gerhard W. 1982. The antigenic structure of the influenza virus A/PR/8/34 hemagglutinin (H1 subtype). Cell 31:417–427. http://dx.doi.org/10.1016/0092-8674(82)90135-0.
11. Gerhard W, Yewdell J, Frankel ME, Webster R. 1981. Antigenic structure of influenza virus haemagglutinin defined by hybridoma antibodies. Nature 290:713–717. http://dx.doi.org/10.1038/290713a0.
12. Garten RJ, Davis CT, Russell CA, Shu B, Lindstrom S, Balish A, Sessions WM, Xu X, Skepner E, Deyde V, Okomo-Adhiambo M, Gubareva L, Barnes J, Smith CB, Emery SL, Hillman MJ, Rivailler P, Smagala J, de Graaf M, Burke DF, Fouchier RA, Pappas C, Alpuche-Aranda CM, Lopez-Gatell H, Olivera H, Lopez I, Myers CA, Faix D, Blair PJ, Yu C, Keene KM, Dotson PD, Jr, Boxrud D, Sambol AR, Abid SH, St George K, Bannerman T, Moore AL, Stringer DJ, Blevins P, Demmler-Harrison GJ, Ginsberg M, Kriner P, Waterman S, Smole S, Guevara HF, Belongia EA, Clark PA, Beatrice ST, Donis R, Katz J, Finelli L, Bridges CB, Shaw M, Jernigan DB, Uyeki TM, Smith DJ, Klimov AI, Cox NJ. 2009. Antigenic and genetic characteristics of swine-origin 2009 A(H1N1) influenza viruses circulating in humans. Science 325:197–201. http://dx.doi.org/10.1126/science.1176225.
13. O'Donnell CD, Vogel L, Wright A, Das SR, Wrammert J, Li GM, McCausland M, Zheng NY, Yewdell JW, Ahmed R, Wilson PC, Subbarao K. 2012. Antibody pressure by a human monoclonal antibody targeting the 2009 pandemic H1N1 virus hemagglutinin drives the emergence of a virus with increased virulence in mice. mBio 3(3):e00120–00112. http://dx.doi.org/10.1128/mBio.00120-12.
14. Rudneva I, Ignatieva A, Timofeeva T, Shilov A, Kushch A, Masalova O, Klimova R, Bovin N, Mochalova L, Kaverin N. 2012. Escape mutants of pandemic influenza A/H1N1 2009 virus: variations in antigenic specificity and receptor affinity of the hemagglutinin. Virus Res. 166:61–67. http://dx.doi.org/10.1016/j.virusres.2012.03.003.
15. Krause JC, Tsibane T, Tumpey TM, Huffman CJ, Basler CF, Crowe JE, Jr. 2011. A broadly neutralizing human monoclonal antibody that recognizes a conserved, novel epitope on the globular head of the influenza H1N1 virus hemagglutinin. J. Virol. 85:10905–10908. http://dx.doi.org/10.1128/JVI.00700-11.
16. Whittle JR, Zhang R, Khurana S, King LR, Manischewitz J, Golding H, Dormitzer PR, Haynes BF, Walter EB, Moody MA, Kepler TB, Liao HX, Harrison SC. 2011. Broadly neutralizing human antibody that recognizes the receptor-binding pocket of influenza virus hemagglutinin. Proc. Natl. Acad. Sci. U. S. A. 108:14216–14221. http://dx.doi.org/10.1073/pnas.1111497108.
17. Nakajima S, Nakajima K, Nobusawa E, Zhao J, Tanaka S, Fukuzawa K. 2007. Comparison of epitope structures of H3HAs through protein modeling of influenza A virus hemagglutinin: mechanism for selection of antigenic variants in the presence of a monoclonal antibody. Microbiol. Immunol. 51:1179–1187. http://dx.doi.org/10.1111/j.1348-0421.2007.tb04013.x.
18. Nobusawa E, Sato K. 2006. Comparison of the mutation rates of human influenza A and B viruses. J. Virol. 80:3675–3678. http://dx.doi.org/10.1128/JVI.80.7.3675-3678.2006.
19. Tsuchiya E, Sugawara K, Hongo S, Matsuzaki Y, Muraki Y, Li ZN, Nakamura K. 2001. Antigenic structure of the haemagglutinin of human influenza A/H2N2 virus. J. Gen. Virol. 82:2475–2484.
20. Lubeck MD, Gerhard W. 1981. Topological mapping antigenic sites on the influenza A/PR/8/34 virus hemagglutinin using monoclonal antibodies. Virology 113:64–72. http://dx.doi.org/10.1016/0042-6822(81)90136-7.
21. Nakajima S, Nishikawa F, Nakajima K. 2000. Comparison of the evolution of recent and late phase of old influenza A (H1N1) viruses. Microbiol. Immunol. 44:841–847. http://dx.doi.org/10.1111/j.1348-0421.2000.tb02572.x.
22. Wei CJ, Boyington JC, Dai K, Houser KV, Pearce MB, Kong WP, Yang ZY, Tumpey TM, Nabel GJ. 2010. Cross-neutralization of 1918 and 2009 influenza viruses: role of glycans in viral evolution and vaccine design. Sci. Transl. Med. 2:24ra21. http://dx.doi.org/10.1126/scitranslmed.3000799.
23. Yang H, Carney P, Stevens J. 2010. Structure and receptor binding properties of a pandemic H1N1 virus hemagglutinin. PLoS Curr. 2:RRN1152. http://dx.doi.org/10.1371/currents.RRN1152.
24. Chen Z, Wang W, Zhou H, Suguitan AL, Jr, Shambaugh C, Kim L, Zhao J, Kemble G, Jin H. 2010. Generation of live attenuated novel influenza virus A/California/7/09 (H1N1) vaccines with high yield in embryonated chicken eggs. J. Virol. 84:44–51. http://dx.doi.org/10.1128/JVI.02106-09.
25. World Health Organization. 2013. Review of the 2012-2013 winter influenza season, northern hemisphere. Wkly. Epidemiol. Rec. 88:225–232.
26. World Health Organization. 2013. Review of the 2013 influenza season in the southern hemisphere. Wkly. Epidemiol. Rec. 88:509–520.
27. Webster RG, Kendal AP, Gerhard W. 1979. Analysis of antigenic drift